11
Coupled Solid–Fluid Problems

We considered a variety of problems in Chaps. 2–10 that fall within the domain of either biosolid mechanics or biofluid mechanics, each of which is very important in its own right. Whether in the body (in vivo) or in the laboratory (in vitro), however, many "real-life" problems simultaneously involve solid–fluid interactions. For example, although we may seek to determine the stresses in the limbs of a pilot who has ejected from an aircraft, for purposes of identifying safety measures, it is the wind that induces the applied loads of importance; most intracranial aneurysms may be considered as thin-walled, nearly spherical membranes that exhibit a solidlike character, but the applied loads are due to the internal flowing blood and the surrounding cerebrospinal fluid; mechanotransduction in bone, which exhibits a strong solidlike behavior, appears to be influenced directly by loads due to weight bearing and those due to the flow of blood and bone fluid within the many different canals within the bone; and an atomic force microscopic examination of the mechanics of a cell may primarily reveal the properties of the cortical membrane and underlying solidlike cytoskeleton, but flow of the cytosol likely plays a key role as well. Hence, from these simple examples, and many more like them, we see that solid–fluid interactions are important at the organism, organ, tissue, cellular, and molecular levels. Indeed, although it tends to be convenient to introduce students to a field by focusing only on one subject, most research and clinical problems require interdisciplinary and multidisciplinary approaches (i.e., analysis and design of *coupled problems*). Such problems are typically complex and require advanced approaches, but here we consider a few introductory examples.

J.D. Humphrey, S.L. O'Rourke, *An Introduction to Biomechanics*,
DOI 10.1007/978-1-4939-2623-7_11

11.1 Vein Mechanobiology

11.1.1 Biological Motivation

The saphenous vein used in a coronary artery bypass surgical procedure (cf. Fig. 3.8 of Chap. 3) will grow and remodel in response to its altered environment, which includes marked changes in pressure and flow. To understand the associated mechanobiology, we must compute the blood-pressure-induced stresses in the wall (i.e., the solid mechanics problem; Sect. 3.4 of Chap. 3) as well as the flow-induced wall shear stresses (i.e., the fluid mechanics problem; Sect. 9.2 of Chap. 9). Here, let us consider a simple problem for which we examine possible morphological changes due to the altered pressure and flow experienced by the vein graft. Consistent with prior analyses, consider as a first approximation the mean circumferential wall stress $\sigma_{\theta\theta}$ due to a quasistatic pressurization and the mean wall shear stress τ_w due to a steady flow.

11.1.2 Theoretical Framework

Let the normal venous pressure and flow be denoted by P (~5 mmHg) and Q (~20 mL/s, where the mean velocity $\overline{v} \sim 0.01 - 0.04\,\mathrm{m/s}$). Moreover, let the arterial values be given by $P_a = \varepsilon_P P$ and $Q_a = \varepsilon_Q Q$, where scaling factors $\varepsilon_P = 120/5 \approx 24$ and $\varepsilon_Q = 40/20 \approx 2$. Hence, in the normal physiologic state, we have [from Eqs. (3.41) and (9.55)]

$$\sigma_{\theta\theta} = \frac{Pa}{b-a}, \quad \tau_w = \frac{4\mu Q}{\pi a^3}, \tag{11.1}$$

where a is the homeostatic pressurized inner radius and $b-a$ is the associated thickness. In the altered (bypass) state, we have

$$\sigma_{\theta\theta} = \frac{(\varepsilon_P P) r_i}{h}, \quad \tau_w = \frac{4\mu(\varepsilon_Q Q)}{\pi r_i^3}, \tag{11.2}$$

where r_i and h are the new (altered) inner radius and wall thickness, respectively. If the vein grows and remodels over time such that it restores the wall shear and circumferential stresses to the basal levels, then

$$\frac{4\mu(\varepsilon_Q Q)}{\pi r_i^3} = \frac{4\mu Q}{\pi a^3}, \quad \frac{(\varepsilon_P P) r_i}{h} = \frac{Pa}{b-a}, \tag{11.3}$$

or

$$r_i = (\varepsilon_Q)^{1/3} a, \quad h = \varepsilon_P (\varepsilon_Q)^{1/3} (b-a). \tag{11.4}$$

Hence, by comparing morphologically measured values of a versus r_i and $b - a$ versus h in terms of the alterations ε_p and ε_Q, we can test the simple hypotheses that the vascular wall grows and remodels in such a way that it restores both $\sigma_{\theta\theta}$ and τ_w to the basal values. Such a hypothesis is teleologically attractive because we expect endothelial cells to function best at a particular value of τ_w and the medial smooth muscle cells to likewise function best at a particular value of $\sigma_{\theta\theta}$. We also expect, of course, that such growth and remodeling will occur over days to weeks or months. For a more complete understanding, therefore, we need to augment Eqs. (11.1) and (11.2), which come from equilibrium and boundary conditions, with constitutive equations that account for the growth and remodeling. As noted in Humphrey (2002), it appears that growth and remodeling is a result of imbalances in the production and removal of constituents at altered configurations. In the case of the vein graft, its configuration will be altered initially by the increased pressure (due to elastic distension and possibly damage-induced weakening) and the increased flow (due to endothelial production of vasodilators to enlarge the lumen and thereby reduce the wall shear stress). Accounting for the altered production and removal of cells and matrix requires kinetic relations in addition to constitutive relations for stress. As noted in Chap. 12, formulation of appropriate kinetic relations for mechanosensitive changes in tissue constituents is one of the most important needs today in biomechanics. In this simple example, therefore, we see how a biomechanical analysis can be used to investigate the mechanobiology, indeed to identify what needs to be measured and why, and that solid and fluid mechanics must be considered simultaneously in certain problems. It should also be noted, however, that whereas Eqs. (11.4) appear to describe well the long-term adaptation of arteries to modest increases or decreases in hemodynamics, vein grafts often do not adapt optimally to arterial conditions. There is a further need, therefore, to understand the limits on biological growth and remodeling that may be imposed by the original genetic programming that led to near optimal behavior of arteries under arterial conditions and veins under venous conditions.

11.2 Diffusion Through a Membrane

11.2.1 Biological Motivation

There are many different types of membranes in the body: plasma membranes which surround/define a cell, the pericardium which surrounds the heart, the pleura which surrounds the lungs, the meninges (i.e., dura mater, pia mater, and arachnoid) which surround the brain, the sheaths that cover tendons, and so on. These membranes serve a variety of biological and mechanical functions. For example, the pericardium appears to restrict gross motions of the heart,

which is otherwise suspended freely within the thorax via its connections to major blood vessels at its base. It is also thought that the pericardium, which exhibits a compliant behavior at low strains but a stiff behavior at high strains (cf. Fig. 2.23 of Chap. 2) tends to limit any acute overdistension of the heart (we emphasize acute, for growth and remodeling of the pericardium allows chronic dilatations of the heart, as in congestive heart failure). Finally, the pericardium encloses the pericardial space, which is filled with a small amount of lubricating fluid that reduces frictional forces between the beating heart and the protective pericardial sac, and it allows for selective transmural diffusion of molecules, particularly water and water-bound substances. There is often a need, therefore, to understand the *permeability* of biological membranes and how the permeability changes with disease, injury, repair, clinical treatment, functional adaptation, and even normal development. Toward this end, let us design a simple experiment to quantify the permeability of a nonlinear biological membrane.

11.2.2 Theoretical Basis

To induce a fluid to flow across a solid membrane, there must be a "driving force" such as a mechanical or a chemical gradient. For simplicity, let us consider the former. Experience reveals that the net flow of a fluid across a thin permeable membrane depends not only on the pressure gradient across the membrane but also on the properties of the fluid, the properties of the membrane, and the thickness of the membrane. In particular, biological membranes typically consist of a monolayer of cells that is attached to a basement membrane that covers an underlying 2-D plexus of structural proteins, which, in turn, are embedded in a proteoglycan-dominated matrix. Hence, the effective *porosity* of the network of fibers plays a key role in defining the overall permeability. This network may change with finite deformations, of course; hence, we also expect the permeability to vary with strain.

Recalling from Chap. 6 that the deformation gradient $[F]$ is the fundamental measure of motion and thus deformation, we ultimately desire to know how changes in $[F]$ affect the permeability. Because $[F]$ may vary from point to point in general (i.e., it can describe nonhomogeneous deformations) and it is defined by nine independent components, it would be prudent to investigate a possible deformation-dependent permeability first in terms of a simple motion. Consider, therefore, a homogenous deformation of a circular membrane that is defined by the mapping of a generic material particle originally at (R, Θ, Z) to (r, θ, z) in a current configuration whereby

$$r = \beta R, \quad \theta = \Theta, \quad z = \lambda Z, \tag{11.5}$$

and β and λ are stretch ratios (i.e., just numbers for each equilibrium state). This mapping reveals that a material particle will not change its circumferential location; it will merely move along a radial line and move up and down as the stretched or unstretched membrane thins and thickens. From Eq. (6.81) of Chap. 6, therefore, the components of $[F]$ are

$$[F] = \begin{bmatrix} \beta & 0 & 0 \\ 0 & \beta & 0 \\ 0 & 0 & \lambda \end{bmatrix}, \tag{11.6}$$

which we see are independent of position (R, Θ, Z) as desired; that is, associated measurements of permeability will reveal the influence of a single stretch, not the average effect of different stretches at different points. Note, too, that the deformation is *equibiaxial* in-plane; that is, the stretch β is the same in the radial and circumferential directions in each equilibrium state. Question: How is this the case if particles move in the radial direction, but not in the circumferential direction? The answer, of course, is that as particles move radially outward, the circumference $2\pi r$ increases and $\beta = 2\pi r/2\pi R = r/R$ (a ratio of lengths) in this homogeneous deformation.

If we further assume that the membrane is mechanically incompressible, then $\det[F] = 1$ and, therefore, $\beta^2\lambda = 1$ or $\beta = 1/\sqrt{\lambda}$. Hence, by simply measuring either the out-of-plane stretch λ or the in-plane equibiaxial stretch β at any point, we can completely quantify the deformation at every point. This clearly simplifies the experimental challenge of quantifying a deformation-dependent permeability and again reveals that theory should guide experiment.

Let us now seek a functional relationship among the net volumetric flow rate Q and the pressure drop Δp, the properties of the fluid (say ρ and μ if Newtonian), the geometry of the membrane (say, initial radius A and thickness H), and the deformation (say, λ); that is, we seek to identify experimentally the specific functional form (recall the acrostic DEICE from Chap. 1) of the relation

$$Q = f(\Delta p, \rho, \mu, A, H, \lambda). \tag{11.7}$$

With six independent variables, such a determination could be very difficult and require many experiments if one tries to hold five of the six variables constant while varying one alone; repeating this process to isolate the effect of each variable could thus result in many, many experiments, each of which would have to be repeated to identify further effects of experimental noise or specimen-to-specimen variation. Thus, let us appeal to the Buckingham Pi (Sect. 10.5 of Chap. 10) approach to address this.

Recalling the five-step recipe for this approach (SCALE), note (Step 2) that fundamental units/dimensions for this isothermal problem are length L, time T, and mass M. Moreover, the units of each variable are as follows:

$$[Q] = \frac{\text{Volume}}{\text{Time}} = L^3T^{-1}M^0,$$
$$[\Delta p] = \frac{\text{Force}}{\text{Area}} = L^{-1}T^{-2}M^1,$$
$$[\rho] = \frac{\text{Mass}}{\text{Volume}} = L^{-3}T^0M^1,$$
$$[\mu] = \frac{\text{Force}/\text{Area}}{1/\text{Time}} = L^{-1}T^{-1}M^1,$$
$$[A] = \text{Length} = L^1T^0M^0,$$
$$[H] = \text{Length} = L^1T^0M^0,$$
$$[\lambda] = \text{Non-dimensional} = L^0T^0M^0.$$

Next (Step 3), we must assign reasonable scales. As noted in Chap. 10, this is the most important step, and experience often serves one well. Nevertheless, we should find comfort in knowing that such selections are not unique and, consequently, one often tries multiple combinations of scales and evaluates the utility of each. Note, therefore, that possible length scales include

$$A,\ a,\ H,\ h, \tag{11.8}$$

where a and h are the deformed radius and thickness, respectively; that is, $a = \beta A$ and $h = \lambda H$. Possible mass scales include

$$\rho a^2 h,\ \rho A^2 H,\ \rho a^3,\ \rho h^3,\ \ldots \tag{11.9}$$

where the mass density (mass/volume) simply needs to be multiplied by a volume term to yield a mass. As usual, the timescale is often more difficult to select. Possible scales include (verify that each is a unit of time) the following:

$$\sqrt{\frac{h}{g}},\quad \sqrt{\frac{\rho A^2}{\Delta p}},\quad \sqrt{\frac{\rho a^2}{\Delta p}},\quad \frac{a^2 h}{Q},\quad \frac{\mu}{\Delta p}; \tag{11.10}$$

that is, we can exploit any quantity having a unit of time, including velocity, acceleration, volumetric flow rate, force (which is a mass times acceleration, which has a unit of time), pressure, and material properties such as viscosity or even a shear modulus.

Rather than comparing this analysis for multiple sets of scales, as we would do in practice, here we illustrate the procedure using scales that are revealed to be useful in hindsight. Hence, let us select the following scales:

$$L_s = A, \quad T_s = \frac{\mu}{\Delta p}, \quad M_s = \rho A^2 H. \tag{11.11}$$

One reason for this selection is that A and H are defined in the undeformed configuration and thus they do not change with the stretch λ or the flow across the membrane. The next step (Step 4) in the Buckingham Pi procedure is to determine the Pi variables. Thus, note that

$$\pi_1 = \frac{Q}{(A)^3(\mu/\Delta p)^{-1}\left(\rho A^2 H\right)^0} = \frac{Q\mu}{\Delta p A^3}, \tag{11.12}$$

$$\pi_2 = \frac{\Delta p}{(A)^{-1}(\mu/\Delta p)^{-2}\left(\rho A^2 H\right)^1} = \frac{\mu^2}{\Delta p \rho A H}, \tag{11.13}$$

$$\pi_3 = \frac{\rho}{(A)^{-3}(\mu/\Delta p)^0\left(\rho A^2 H\right)^1} = \frac{A}{H}, \tag{11.14}$$

$$\pi_4 = \frac{\mu}{(A)^{-1}(\mu/\Delta p)^{-1}\left(\rho A^2 H\right)^1} = \frac{\mu^2}{\Delta p \rho A H}, \tag{11.15}$$

$$\pi_5 = \frac{A}{(A)^1(\mu/\Delta p)^0\left(\rho A^2 H\right)^0} = 1, \tag{11.16}$$

$$\pi_6 = \frac{H}{(A)^1(\mu/\Delta p)^0\left(\rho A^2 H\right)^0} = \frac{H}{A} = \frac{1}{A/H}, \tag{11.17}$$

$$\pi_7 = \lambda. \tag{11.18}$$

Noting that our six original independent variables have been reduced to three independent variables, the final step (Step 5) in the Buckingham Pi procedure yields

$$Q = f(\Delta p, \rho, \mu, A, H, \lambda) \rightarrow \pi_1 = \widetilde{f}(\pi_2, \pi_3, \pi_7), \tag{11.19}$$

or

$$\frac{Q\mu}{\Delta pA^3} = \widetilde{f}\left(\frac{\mu^2}{\Delta p\rho AH}, \frac{A}{H}, \lambda\right). \tag{11.20}$$

Experimental determination of this relation in terms of three dependent variables certainly has greater promise than that for the original relation, which has six dependent variables. For example, if we are interested primarily in the flow of a particular fluid (e.g., interstitial fluid or pericardial fluid) as a function of the pressure gradient and stretch, then we would simply need to vary π_2 and π_7 for a convenient value of π_3.

11.2.3 Illustration

Studies of diffusion through various materials, including biomembranes, are often based on the so-called *Darcy's law*, which was put forth by H. P. Darcy in 1856 based on the flow of water through soil. Darcy, a French civil engineer, was given the task of providing the city of Dijon with clean water. To do this, he created an elaborate underground aqueduct system; in 1856, he published a paper describing his design process, which included an appendix describing how sand can filter water. Regardless, Darcy's law is often stated in the following form:

$$\frac{Q}{\pi a^2} = \frac{k}{\mu}\left(\frac{\Delta p}{h}\right), \tag{11.21}$$

where πa^2 and h are the current surface area and the thickness, respectively, of the material through which the fluid flows and k is a *permeability coefficient* (having units of length squared). In the special case of no strain of the solid (i.e., $a \equiv A$ and $h \equiv H$), therefore, Darcy's law can be rewritten as

$$\frac{Q\mu}{\Delta pA^3} = K\left(\frac{A}{H}\right) \tag{11.22}$$

where

$$K = \frac{k\pi}{A^2}.$$

Comparison of this relation with Eq. (11.20) reveals that Darcy's law is a special case of our general relation whereby $\widetilde{f} = (K)(A/H)$ and K is a nondimensional permeability; that is, Darcy's law requires that $\widetilde{f}$ depend linearly on π_3 and be independent of π_2, with $\pi_7 \equiv 1$ for no strain. Use of the

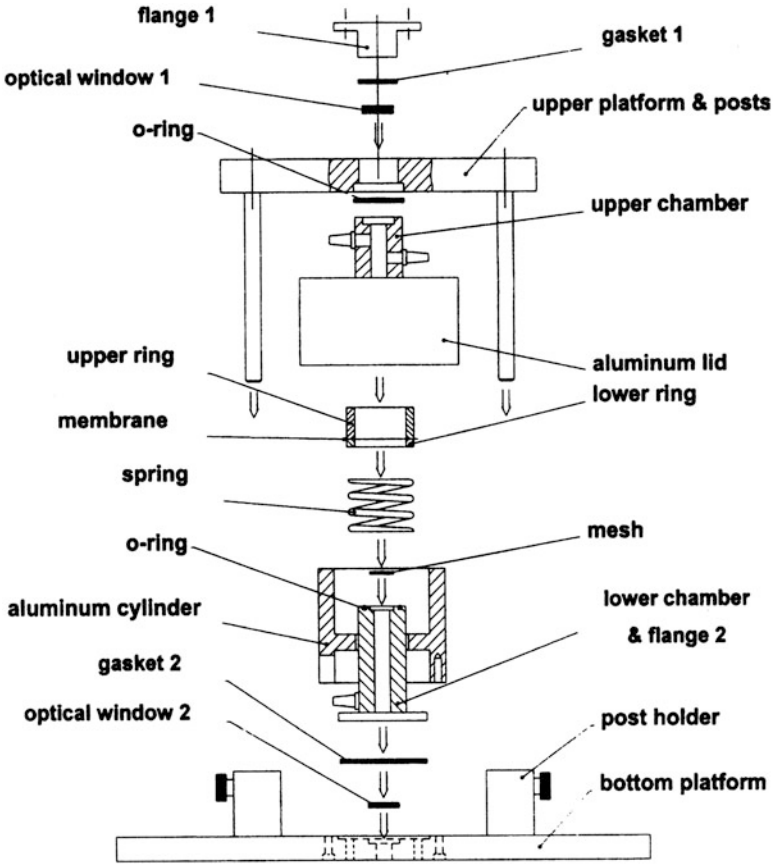

FIGURE 11.1 Exploded view of the combined stretching-diffusion device designed, in part, by Janna Vaughn as part of a senior project at Texas A&M University. From Vaughn et al. (2002), with permission from Elsevier Science.

more general result from Buckingham Pi is preferred, however, because it does not presuppose a specific functional form.

For a senior project at Texas A&M University, Janna Vaughn (see Vaughn et al. 2002) used a Buckingham-Pi-based approach to guide the design of a device to study the strain-dependent permeability of a representative biomembrane—excised bovine epicardium (which was obtained from a abattoir). Figure 11.1 is an exploded view of the combined stretching-diffusion device. Briefly, a membrane is first mounted in a stress-free configuration between two circular fixtures (Fig. 11.2) and then placed in the device between the upper and lower fluid-filled chambers. A nearly uniform equibiaxial stretch β of the specimen is imposed by pushing the specimen fixture down such that

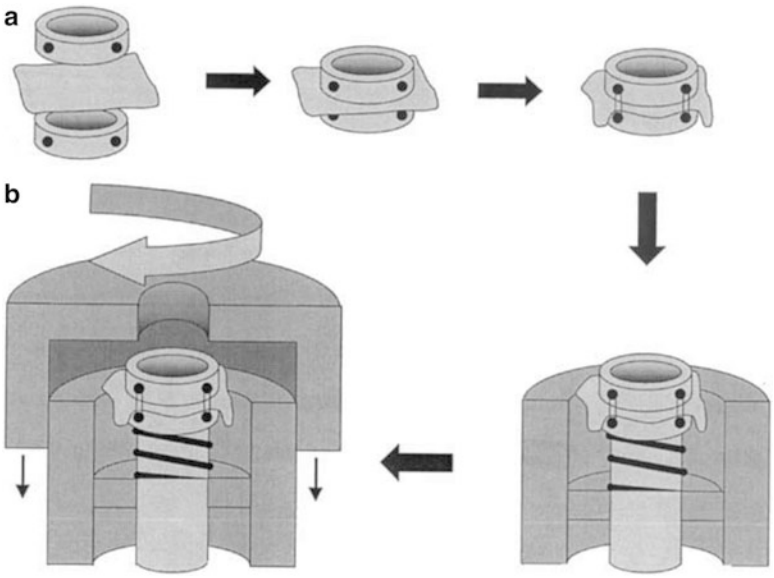

FIGURE 11.2 Expanded view of the specimen fixture from Fig. 11.1. Note that the specimen is placed within the fixture in a stress-free configuration (Panel *a*). This is facilitated by having a waxed platform inside the restraining rings on which a fluid film can support the specimen prior to mounting. Turning the outer lid pushes down on the membrane holder, which, in turn, imposes a uniform radial stretch of the specimen (Panel *b*). With permission from Elsevier Science.

the specimen is pulled over the outer surface of the bottom chamber (this is akin to pulling a rubber membrane over a tube to create a drum); this is accomplished by turning a threaded aluminum lid above the upper chamber that pushes the specimen holder down. Also above the upper chamber is an upper platform that applies an overall compressive load to the upper and lower chambers; O-rings ensure a good seal. Fluid flows into the upper chamber, through the membrane, and out of the lower chamber via appropriate fittings. Finally, note that optical windows at the bottom and top allow back-lighting and visualization of markers that are affixed to the surface of the specimen. Tracking the motions of these markers due to stretching of the membrane allows the displacements and their gradients to be computed (Chap. 2).

Figures 11.3 and 11.4 show data from Janna's experiments wherein π_1 is plotted versus π_2 and π_7 $(=\lambda)$, for different values of π_7 and π_2, respectively. Over the range of parameters studied, π_1 varied with π_7 much more than it did with π_2, which is not explained by Darcy's law. Indeed, plotting the data as the nondimensional permeability K versus stretch λ (Fig. 11.5) reveals a strong strain dependency. That K increased with increasing stretch may suggest that

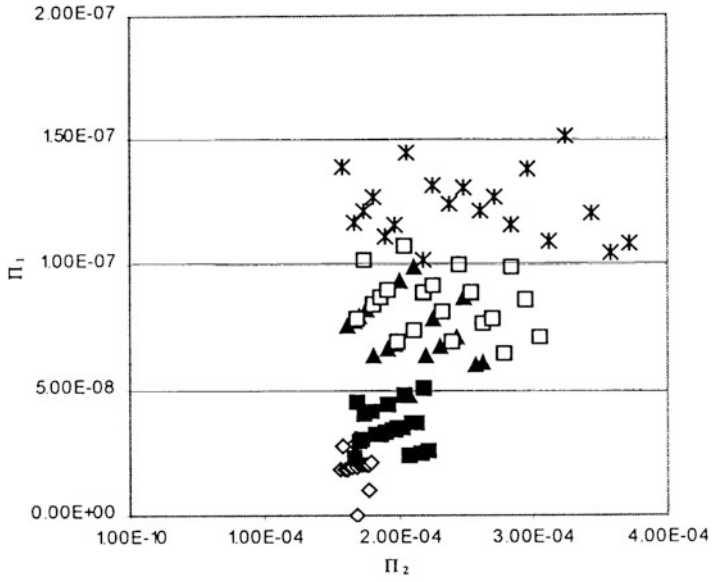

FIGURE 11.3 Data for two of the nondimensional parameters from Eq. (11.20): π_1 versus π_2 for various values of π_7 (denoted by *open diamonds*, *closed squares*, *closed triangles*, *open squares*, and *asterisks* for increasing levels of stretch from 1.0 to 1.6, clearly finite deformations). With permission from Elsevier Science.

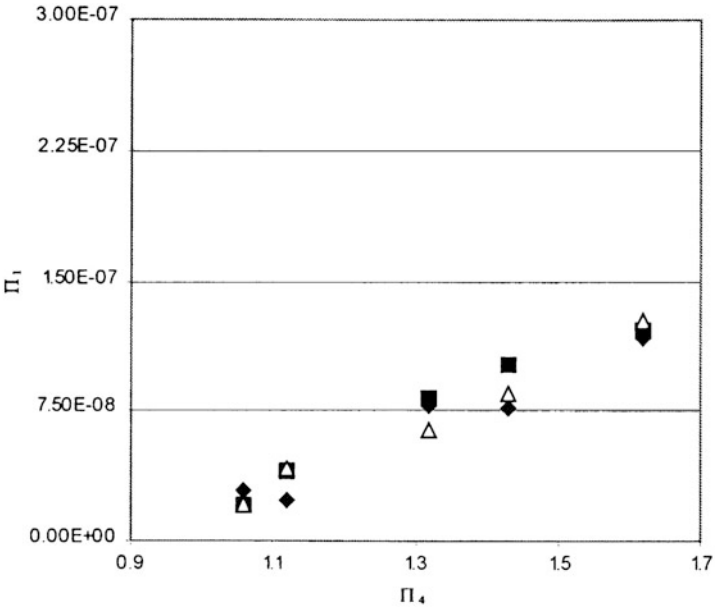

FIGURE 11.4 Similar to Fig. 11.3 except for π_1 versus π_7 for various values of π_2 over the range in Fig. 11.3. Note that π_7 was denoted as π_4 in the original paper. With permission from Elsevier Science.

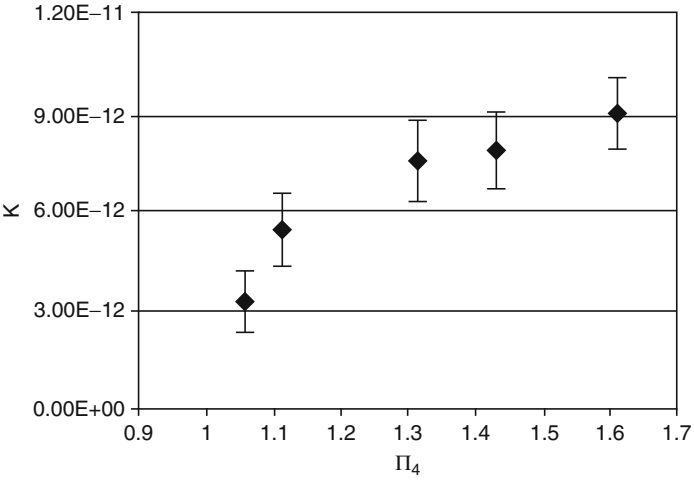

FIGURE 11.5 Similar to Figs. 11.3 and 11.4 except for the nondimensional permeability K versus the equibiaxial stretch λ. With permission from Elsevier Science.

stretching brings the collagenous fibers closer together, compacting the tissue and thus increasing the resistance to flow. More experiments and analyses are needed to understand this complex solid–fluid coupling, however.

In closing, note that the Δp in this formulation represents the pressure difference across the membrane (Fig. 11.1). Although it is difficult to measure directly the pressure at these surfaces during flow, the pipe-flow equation [Eq. (10.94) of Chap. 10] can be used to compute p_1 and p_2 based on pressures measured elsewhere in the system (e.g., atmospheric pressure in an open upstream reservoir), differences in height, velocities, and viscous and geometric losses. Indeed, one would use the pipe-flow equation twice: once to get the difference between the pressure at its source and that value at the top surface of the membrane, and once to get the difference between the pressure at the bottom surface of the membrane and that at the ultimate exit point. Hence, as implied in Chap. 10, the pipe-flow equation can be very useful in the design and analysis of important biomechanical experiments. For very slow flows, of course, the system is nearly quasistatic and pressure differences would be due primarily to the gravitational heads ρgh. In general, however, the full pipe-flow equation should be checked to determine the specific values of velocity for which the quasistatic assumption is reasonable.

Example 11.1 In Sect. 11.1, we considered a simple case of fluid-solid coupling in the vasculature—effects of steady blood flow Q and pressure P on wall shear stress and intramural stress in veins and associated

mechanobiological implications. Perhaps the simplest consideration of effects of wall properties on blood flow in arteries is embodied in the Moens-Korteweg equation (derived by T. Young in 1808); it relates the speed of propagation of a pressure wave in an inviscid fluid that is contained within a long, uniform thickness and diameter circular tube that exhibits a linearly elastic response. Albeit now known to be theoretically inappropriate in vascular mechanics, this simple equation helps one to build some intuition nonetheless. Following Ethier and Simmons (2007), use dimensional analysis to find this famous result.

Solution: Assume that the speed c of an arterial pressure wave depends on the gross mechanical properties of both the artery, via its distensibility D, and the blood, via its mass density ρ. That is, let $c = f(D, \rho)$ where $D = (d_{sys} - d_{dias})/(P_{sys} - P_{dias})d_{dias}$, with d the diameter and P the pressure at either sys(tole) or dias(tole). Following methods introduced in Sect. 10.5, note that the dimensions of our primary variables are:

$$[c] = L^1T^{-1}M^0, \qquad [D] = L^1T^2M^{-1}, \qquad [\rho] = L^{-3}T^0M^1.$$

Now, if we assign length, time, and mass scales as

$$L_s = d, \qquad T_s = d/c, \qquad M_s = \rho d^3,$$

then our Pi groups become,

$$\pi_c = c/c = 1, \qquad \pi_D = D/\left(\rho c^2\right)^{-1} = \rho c^2 D, \qquad \pi_\rho = \rho/\rho = 1.$$

Hence, our final result is $1 = f(\rho c^2 D, 1)$, which implies that $\rho c^2 D = \text{constant}$. Simple experiments using a long, constant diameter and thickness, circular, stiff tube containing a low viscosity fluid suggest that this constant is ~½. The final result, therefore, is

$$\rho c^2 D = ½ \quad \text{or} \quad c^2 = 1/2\rho D.$$

Early investigators sought, however, to rewrite this result in terms of the material stiffness (e.g., Young's modulus E of linearized elasticity) instead of the gross structural stiffness (distensibility D). Recalling from Eq. (3.41) that the circumferential stress in a thin-walled pressurized cylindrical tube of diameter d and thickness h is $\sigma = Pd/2h$ and that for a simple 1-D linearly elastic behavior $\sigma = E\varepsilon$ [cf. Eq. (2.69)], it was then assumed that an increment in stress $\Delta\sigma = \Delta Pd/2h$ (from diastole to systole, relative to diastole) was related to an increment in strain $\Delta\varepsilon = (d_{sys} - d_{dias})/d_{dias}$ (relative to diastole), whereby $\Delta\varepsilon = \Delta\sigma/E = \Delta Pd/2Eh$ as well as (from above) $\Delta\varepsilon = D\Delta P$. Hence, using our non-dimensional result, we have $D\Delta P = \Delta P/2\rho c^2$ and using our equilibrium

result we have $\Delta Pd/2Eh$, which when combined yields $c^2 = Eh/\rho d = Eh/2\rho a$, where a is the radius of the tube. Hence, the Moens-Korteweg prediction of the speed of the pressure wave can be written

$$c = \sqrt{\frac{Eh}{2\rho a}}$$

In other words, the speed of propagation of a pressure wave in an inviscid fluid contained within a linearly elastic thin-walled tube is expected to increase with an increase in either the material stiffness (e.g., E) or the structural stiffness (Eh) of the tube, but to decrease with an increase in either the fluid density (ρ) or the luminal caliber (a). Indeed, in the limit as the stiffness becomes infinite (i.e. the tube becomes rigid), the wave speed also becomes infinite. An infinite wave speed implies that changes in pressure are transmitted instantly to every point within the tube, which essentially suggests a "bulk motion" whereby the entire fluid moves in unison. See Zamir (2000) for a more detailed discussion of the effects of wall elasticity on fluid-solid interactions in unsteady flows, which in the vasculature includes the effects of waves reflecting from sites of geometric (e.g., bifurcations) or material (e.g., synthetic grafts) discontinuities. For example, it is the elasticity of the wall that sustains wave motions in tubes, hence wave reflections do not exist in rigid tubes. Moreover, the viscosity of the fluid (which is neglected in the Moens-Korteweg derivation) tends to attenuate both the speed and amplitude of a traveling wave and thus must be included in vascular mechanics.

Observation 11.1. A commonly studied ordinary differential equation in nonlinear dynamics is the so-called *Duffing equation*. It can be written

$$\eta^2\ddot{x} + cx + \alpha x^3 + 2\eta\zeta\dot{x} = F(t),$$

where η is the ratio of the forcing and fundamental frequencies, c is a stiffness parameter, α is a nonlinear stiffness parameter, and ζ is the ratio of the actual to the critical damping in the system; x, of course, is the displacement and $F(t)$ is the time-varying forcing function. An overdot implies differentiation with respect to time and a double overdot implies twice differentiation with time. To solve this second-order equation numerically (e.g., via Runge–Kutta), it is useful to rewrite it as a system of first-order equations. Toward this end, consider a change of variables whereby

$$y_0 \equiv x \quad \text{and} \quad y_1 \equiv \dot{x}$$

and, consequently,

$$\dot{y}_0 \equiv \dot{x} \quad \text{and} \quad \dot{y}_1 \equiv \ddot{x}.$$

We see, therefore, that our system of first-order equations is

$$\dot{y}_0 = \dot{x},$$
$$\dot{y}_1 = \ddot{x} \equiv \frac{F(t) - cx - \alpha x^3 - 2\eta\zeta\dot{x}}{\eta^2},$$

or in terms of (y_0, y_1) alone,

$$\dot{y}_0 = y_1,$$
$$\dot{y}_1 = \frac{F(t) - cy_0 - \alpha y_0^3 - 2\eta\zeta y_1}{\eta^2}.$$

Hence, we have differential equations of the form

$$\dot{y}_0 = G(y_0, y_1) \quad \text{and} \quad \dot{y}_1 = H(y_0, y_1)$$

where G and H are known functions. This system of equations is nonlinear in y_0 if $\alpha \neq 0$.

Whereas we consider a few numerical solutions below for the full nonlinear system, it is useful to note that qualitative information on the *stability* of the nonlinear system can sometimes be gained by linearizing the system about various equilibria; that is, as in Chap. 5 on the stability of beam columns, we can ask whether the structure would return to its prior equilibrium position if perturbed slightly. It is useful to note, therefore, the following (cf. Figs. 5.21 and 5.22):

If the linearized system is asymptotically stable, then the associated nonlinear system is stable about the chosen equilibrium (or fixed) point.
If the linearized system is neutrally stable, then the linearized solution does not provide any useful information about the nonlinear system.
If the linearized system is unstable about a fixed point, then the associated nonlinear system is likewise unstable about that fixed point although it could stabilize about another equilibrium position.

For the Duffing equation, let an equilibrium position (i.e., fixed point) be denoted by a position λ and a zero velocity; that is, $(x, \dot{x}) = (\lambda, 0) = (y_0, y_1)$ at a constant force $F(t) = F_\lambda$. Hence, linearizing the system of first-order equations about the fixed point can be accomplished using a *Taylor series*, namely

$$\dot{y}_0 = G(\lambda,0) + \left.\frac{\partial G}{\partial y_0}\right|_{(\lambda,0)}(y_0-\lambda) + \left.\frac{\partial G}{\partial y_1}\right|_{(\lambda,0)}(y_1-0) + \text{H.O.T.},$$
$$\dot{y}_1 = H(\lambda,0) + \left.\frac{\partial H}{\partial y_0}\right|_{(\lambda,0)}(y_0-\lambda) + \left.\frac{\partial H}{\partial y_1}\right|_{(\lambda,0)}(y_1-0) + \text{H.O.T.},$$

where H.O.T. stands for higher-order terms, which are neglected in the process of linearization. For our specific system,

$$\frac{\partial G}{\partial y_0} = 0, \qquad \frac{\partial G}{\partial y_1} = 1,$$
$$\frac{\partial H}{\partial y_0} = \frac{-c-3\alpha y_0^2}{\eta^2}, \qquad \frac{\partial H}{\partial y_1} = \frac{-2\zeta}{\eta};$$

thus, with $G(\lambda,\ 0)=0$ and $H(\lambda,\ 0)=0$, the latter because $F_\lambda = c\lambda + \alpha\lambda^3$ at equilibrium, we have

$$\dot{y}_0 = 0(y_0-\lambda) + 1(y_1-0),$$
$$\dot{y}_1 = \frac{-c-3\alpha\lambda^2}{\eta^2}(y_0-\lambda) - \frac{2\zeta}{\eta}(y_1-0),$$

which can be written in matrix form as

$$\begin{Bmatrix} \dot{y}_0 \\ \dot{y}_1 \end{Bmatrix} = \begin{bmatrix} 0 & 1 \\ \dfrac{-c-3\alpha\lambda^2}{\eta^2} & \dfrac{-2\zeta}{\eta} \end{bmatrix} \begin{Bmatrix} y_0-\lambda \\ y_1 \end{Bmatrix}.$$

It can be shown (Strang 1986) that asymptotic stability in the small requires that tr[ ] < 0 *and* det[ ] > 0; alternatively, neutral stability is given by tr[ ] = 0 and det[ ] > 0 *or* by tr[ ] < 0 and det[ ] = 0; finally, an instability about a fixed point is thus given by tr[ ] > 0 *or* det[ ] < 0. Here, of course, tr[ ] and det[ ] denote the trace and determinant, respectively, of the 2×2 matrix [ ] as noted in Appendix 6 of Chap. 6. Clearly, for our system, the trace (i.e., sum of the diagonals) and determinant are

$$\text{tr}[\ ] = \frac{-2\zeta}{\eta}, \quad \det[\ ] = \frac{c+3\alpha\lambda^2}{\eta^2} \quad \forall\lambda,$$

respectively. We see, for example, that stability requires that ζ be nonzero and that ζ and η be of the same sign. If, on the other hand, $\zeta = 0$, the system will be only neutrally stable and the linearization will provide no useful information on the nonlinear system. Let us now consider a few numerical examples of the full nonlinear system, which can be interpreted with this backdrop.

Example 11.2 Examine the dynamic behavior of a Duffing system with the following values of the numerical parameters: $\eta = 0.0625$, $c = 1.0$, $\alpha = 0$, and $\zeta = 0.1$, with $F(t) = 1.0 \sin t$. Note that this is a linear system because $\alpha = 0$.

Solution: The behavior is best studied graphically in terms of the computed displacement and velocity histories $x(t)$ and $\dot{x}(t)$ as well as the phase-plane plot, $\dot{x}(t)$ versus $x(t)$. This is the so-called geometric method of Poincaré. We use a standard Runge–Kutta numerical method to obtain the solution, which requires that we specify the initial conditions. Here, let the initial conditions be perturbed slightly from equilibrium: $x(0) = 0$ and $\dot{x}(0) = 0.01$. Figure 11.6 reveals the periodic response (i.e., position) given the sinusoidal forcing function. Note, too, that the system recovers quickly from the initial disturbance as expected based on the linearized analysis.

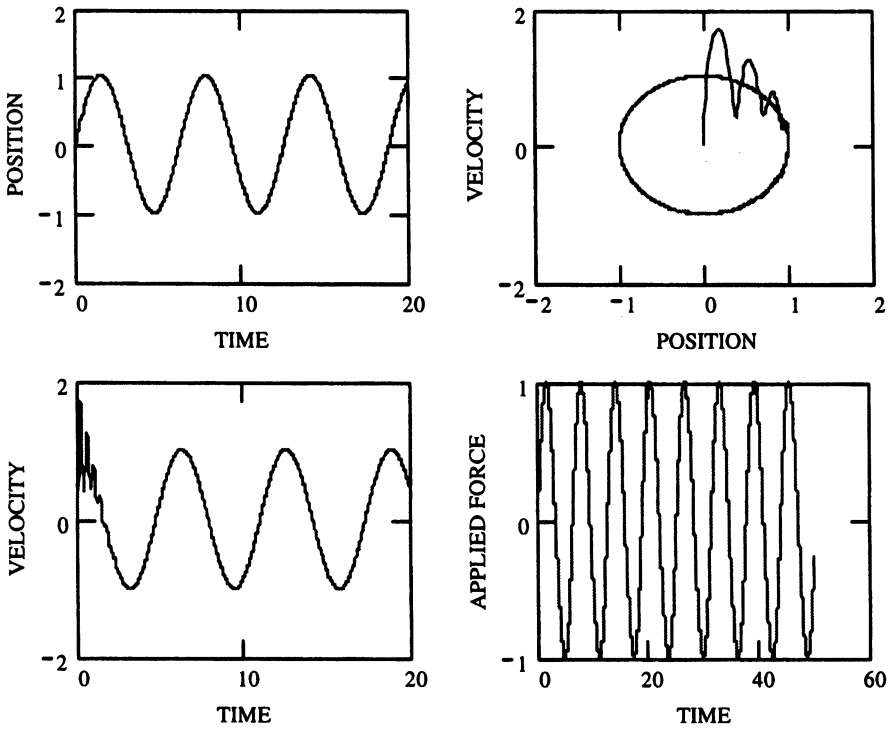

FIGURE 11.6 Results for the Duffing equation ($\alpha = 0$). The *upper left panel* shows position versus time and the *lower left panel* shows velocity versus time, both in response to the forcing function shown in the *bottom right panel*. Finally, the *panel* in the *upper right* shows the so-called *phase-plane diagram*, velocity versus position. It is seen that the response, starting at $(x, \dot{x}) = (0, 0.01)$ quickly finds the so-called periodic solution, revealed by the circular path in the phase plane.

Example 11.3 Repeat the previous example except for a nonlinear case whereby $\alpha = 0.5$. Given that such solutions depend strongly on the initial conditions, also let $x(0) = 0.0$ and $\dot{x}(0) = 1.0$.

Solution: Figure 11.7 shows the results for $\alpha = 0.5$, $x(0) = 0$, and $\dot{x}(0) = 0.01$. Note the differences with respect to Figure 11.6, but the qualitative similarity. Figure 11.8 shows the dramatic effect of the initial condition, now with $x(0) = 1.0$ and $\dot{x}(0) = 1.0$. In both cases, the response is stable, returning to the periodic solution again consistent with the linearization.

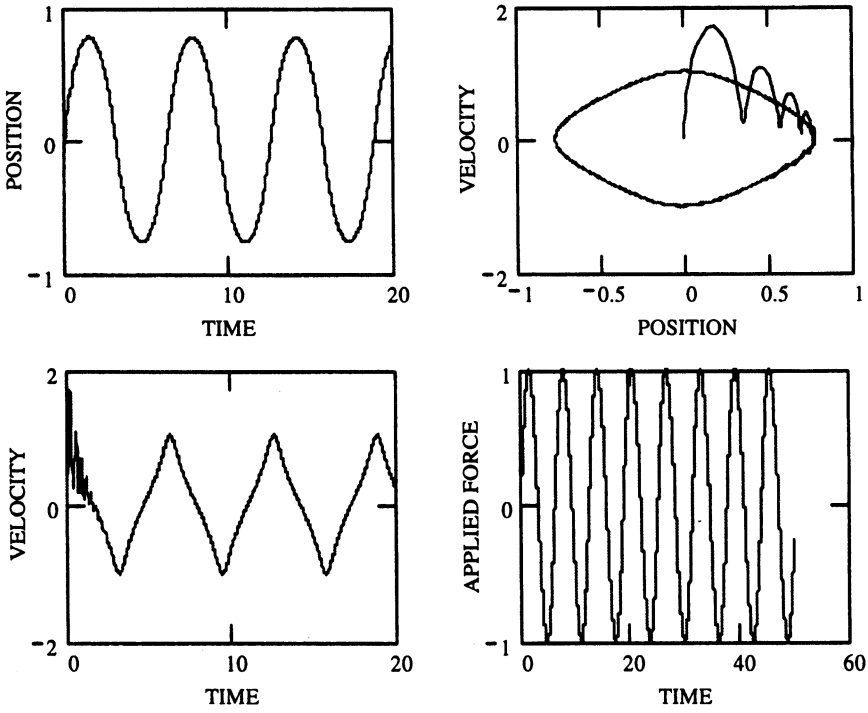

FIGURE 11.7 Similar to Fig. 11.6 except that $\alpha = 0.5$, which induces a nonlinearity.

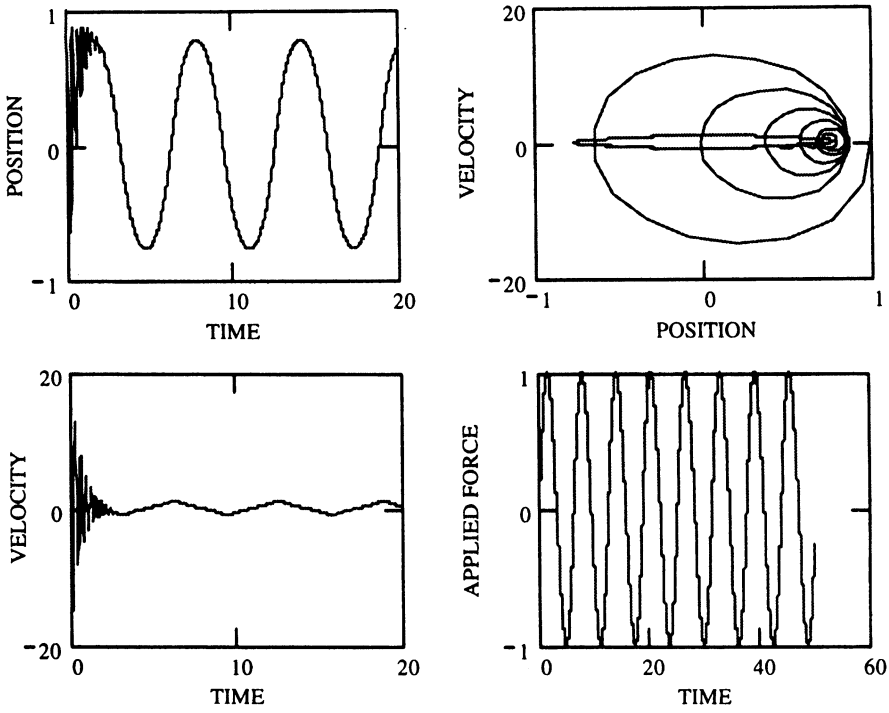

FIGURE 11.8 Similar to Fig. 11.6 except that $\alpha = 0.5$ as well as perturbed initial conditions given by $x(0) = 1.0$ and $\dot{x}(0) = 1.0$.

11.3 Dynamics of a Saccular Aneurysm

11.3.1 Biological Motivation

Recall from Sect. 3.5.1 of Chap. 3 that intracranial saccular aneurysms are thin-walled, balloonlike dilatations of the arterial wall that occur in or near bifurcations in the circle of Willis (Fig. 1.1 of Chap. 1). Based on quasistatic stress analyses, it appears that the intramural wall stress is often on the order of 1 MPa or more, with the rupture strength on the order of 10 MPa. Slight changes in wall thickness or protease degradation of structural proteins within the wall can thereby render these lesions susceptible to rupture. There is a need, therefore, to understand better the solid mechanics of the wall of an aneurysm.

It has been suggested that aneurysms may enlarge or rupture due to a dynamic instability called *resonance*. In particular, some investigators have suggested that the pulsatility of the blood pressure may excite a lesion at its natural frequency and thus induce violent vibrations (i.e., resonance). Whereas the heart-induced blood pressure serves as the forcing function for the lesion, the surrounding cerebrospinal fluid (CSF) may affect the dynamic response of

the lesion as well; that is, as the aneurysm displaces within the CSF due to the distending blood pressure, by Newton's third law the CSF "pushes back." Toward a better understanding of the solid–fluid coupling related to aneurysm dynamics, let us now consider an idealized case: the pressure-induced distension of a spherical lesion that is surrounded by an external CSF.

11.3.2 Mathematical Framework

It can be shown that the equation of motion (i.e., $\boldsymbol{F} = m\boldsymbol{a}$) for a *spherical membrane* can be written as (Humphrey 2002)

$$\sigma_{rr}(b) - \sigma_{rr}(a) - 2T\kappa = \rho_s h \frac{d^2 u_r}{dt^2}, \tag{11.23}$$

where $\sigma_{rr}(b)$ and $\sigma_{rr}(a)$ are the stress boundary conditions on the outer and inner surfaces of the membrane, respectively, T is the membrane tension ($T = h\sigma_{\theta\theta} = h\sigma_{\phi\phi}$, where h is the deformed thickness), κ is the curvature ($\kappa = 1/a$, where a is the deformed radius of the sphere), ρ_s is the mass density of the solid (i.e., the membrane), and $u_r(t) = a(t) - A$ is the radial displacement of any point on the aneurysm (with A the undeformed radius). Note that in the absence of dynamic effects, with $\sigma_{rr}(b) = -P_o$ and $\sigma_{rr}(a) = -\mathrm{P}_i$ the static pressures, Eq. (11.23) recovers the equilibrium solution [Eq. (6.62) of Chap. 6], namely

$$2T\kappa = \sigma_{rr}(b) - \sigma_{rr}(a) \rightarrow 2h\sigma_{\theta\theta}(1/a) = P_i - P_o, \tag{11.24}$$

or

$$\sigma_{\theta\theta} = \frac{(P_i - P_o)a}{2h} \leftrightarrow T = \frac{Pa}{2}, \tag{11.25}$$

where $P = P_i - P_o$ is the transmural pressure. Note, too, that the wall tension T depends on the deformation of the membrane through its constitutive relation. Here, we let the deformation be tracked via the stretch ratio $\lambda(t) = a(t)/A$, a ratio of deformed to undeformed radii [actually, the ratio of deformed to undeformed circumferences, $2\pi a(t)/2\pi A(t)$ for both the θ and ϕ directions]. If the membrane conserves its volume during deformations, then

$$\left(4\pi a^2\right)h = 4\pi A^2 H \rightarrow \frac{h}{H} = \frac{1}{(a/A)^2} = \frac{1}{\lambda^2}, \tag{11.26}$$

where H is the undeformed wall thickness. Show that this is consistent with $\det [F] = 1$, where $[F] = \mathrm{diag}[\lambda, \lambda, h/H]$.

We will assume that the boundary condition on stress at the inner wall is given by the time-varying blood pressure, namely

$$\sigma_{rr}(a,t) = -P_i(t), \quad P_i(t) = P_m + \sum_{n=1}^{N} [A_n \cos(n\omega t) + B_n \sin(n\omega t)], \quad (11.27)$$

consistent with the formulation in Sect. 9.5 of Chap. 9 whereby we recall that P_m is the mean blood pressure, A_n and B_n are Fourier coefficients, and ω is the fundamental circular frequency of the beating heart. To find the outer stress boundary condition, however, we will assume that the CSF is an incompressible, Newtonian fluid. Hence, we need to determine the radial stress in the fluid {recall the Navier–Poisson relation [Eq. (7.65)]},

$$\sigma_{rr}(r,t) = -p(r,t) + 2\mu D_{rr}(r,t), \quad (11.28)$$

which for spherical coordinates is [see Eq. (7.60)]

$$\sigma_{rr}(r,t) = -p(r,t) + 2\mu \frac{\partial v_r}{\partial r} \quad r \in [a,\infty), \quad (11.29)$$

where r is a coordinate in the fluid domain (Fig. 11.9; note, too, that because we are modeling the aneurysm as a membrane, we assume that $b = a + h$, where $h \ll 1$, and thus $a \sim b$). By finding the fluid pressure and velocity fields at all r and time t, we can evaluate the stress exerted by the CSF on the membrane and then solve the solid mechanics problem as desired. To solve the CSF problem, therefore, let us assume the following:

1. Incompressible flow ($\nabla \cdot \boldsymbol{v} = 0$)
2. Newtonian fluid ($\mu = \text{constant}$)
3. Radial unsteady flow only [$v_\theta = 0$, $v_\phi = 0$, $v_r = v_r(r,t)$]
4. Axisymmetric flow ($\partial/\partial\theta = 0$, $\partial/\partial\phi = 0$)
5. Negligible body forces ($\boldsymbol{g} = \boldsymbol{0}$)

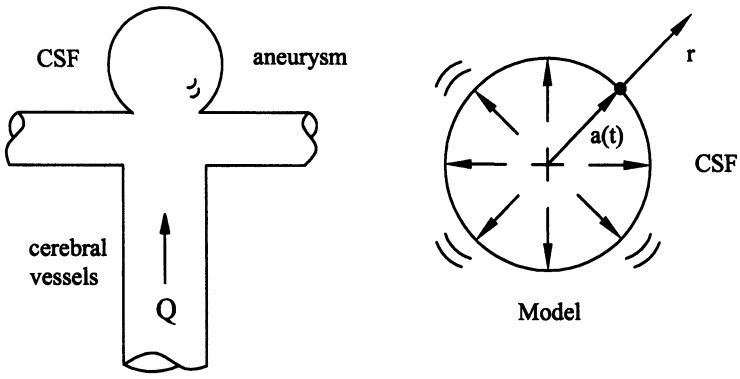

FIGURE 11.9 Simple geometry of a spherical saccular aneurysm surrounded by a fluid that also occupies a spherical domain.

Mass balance in spherical coordinates is [Eq. (8.16)]

$$\frac{1}{r^2}\frac{\partial(r^2 v_r)}{\partial r}+\frac{1}{r\sin\theta}\frac{\partial(v_\theta\sin\theta)}{\partial\theta}+\frac{1}{r\sin\theta}\frac{\partial v_\phi}{\partial\phi}=0. \tag{11.30}$$

In spherical coordinates, the appropriate linear momentum balance equation (i.e., the Navier–Stokes equation, $-\nabla p+\mu\nabla^2\boldsymbol{v}+\rho\boldsymbol{g}=\rho\boldsymbol{a}$) requires the following:

$$\begin{aligned}\hat{\boldsymbol{e}}_r:\quad &-\frac{\partial p}{\partial r}+\mu\left(\nabla^2 v_r-\frac{2v_r}{r^2}-\frac{2}{r^2}\frac{\partial v_\theta}{\partial\theta}-\frac{2v_\theta\cot\theta}{r^2}-\frac{2}{r^2\sin\theta}\frac{\partial v_\phi}{\partial\phi}\right)+\rho g_r\\ &=\rho\left(\frac{\partial v_r}{\partial t}+v_r\frac{\partial v_r}{\partial r}+\frac{v_\theta}{r}\frac{\partial v_r}{\partial\theta}+\frac{v_\phi}{r\sin\theta}\frac{\partial v_r}{\partial\phi}-\frac{v_\theta^2+v_\phi^2}{r}\right),\end{aligned} \tag{11.31}$$

$$\begin{aligned}\hat{\boldsymbol{e}}_\theta:\quad &-\frac{1}{r}\frac{\partial p}{\partial\theta}+\mu\left(\nabla^2 v_\theta+\frac{2}{r^2}\frac{\partial v_r}{\partial\theta}-\frac{v_\theta}{r^2\sin^2\theta}-\frac{2\cos\theta}{r^2\sin\theta}\frac{\partial v_\phi}{\partial\phi}\right)+\rho g_\theta\\ &=\rho\left(\frac{\partial v_\theta}{\partial t}+v_r\frac{\partial v_\theta}{\partial r}+\frac{v_\theta}{r}\frac{\partial v_\theta}{\partial\theta}+\frac{v_\phi}{r\sin\theta}\frac{\partial v_\theta}{\partial\phi}+\frac{v_r v_\theta}{r}-\frac{v_\phi^2\cot\theta}{r}\right),\end{aligned} \tag{11.32}$$

$$\begin{aligned}\hat{\boldsymbol{e}}_\phi:\quad &-\frac{1}{r\sin\theta}\frac{\partial p}{\partial\phi}+\mu\left(\nabla^2 v_\phi-\frac{v_\phi}{r^2\sin^2\theta}+\frac{2}{r^2\sin^2\theta}\frac{\partial v_r}{\partial\phi}+\frac{2\cos\theta}{r^2\sin\theta}\frac{\partial v_\theta}{\partial\phi}\right)+\rho g_\phi\\ &=\rho\left(\frac{\partial v_\phi}{\partial t}+v_r\frac{\partial v_\phi}{\partial r}+\frac{v_\theta}{r}\frac{\partial v_\phi}{\partial\theta}+\frac{v_\phi}{r\sin\theta}\frac{\partial v_\phi}{\partial\phi}+\frac{v_\phi v_r}{r}+\frac{v_\phi v_\theta}{r}\cot\theta\right),\end{aligned} \tag{11.33}$$

where

$$\nabla^2=\frac{1}{r^2}\frac{\partial}{\partial r}\left(r^2\frac{\partial}{\partial r}\right)+\frac{1}{r^2\sin\theta}\frac{\partial}{\partial\theta}\left(\sin\theta\frac{\partial}{\partial\theta}\right)+\frac{1}{r^2\sin^2\theta}\frac{\partial^2}{\partial\phi^2}. \tag{11.34}$$

After canceling out terms using the above assumptions (do it), we are left with

$$\frac{1}{r^2}\frac{\partial}{\partial r}\left(r^2 v_r\right)=0\rightarrow v_r(r,t)=\frac{g(t)}{r^2} \tag{11.35}$$

from mass balance, where $g(t)$ is an arbitrary function due to integration (Note: we have an *integration function* rather than an integration constant because the velocity can depend on both position and time) and

$$-\frac{1}{\rho}\frac{\partial p}{\partial r}+\frac{\mu}{\rho}\left(\nabla^2 v_r-\frac{2v_r}{r^2}\right)=\frac{\partial v_r}{\partial t}+v_r\frac{\partial v_r}{\partial r}, \tag{11.36}$$

from linear momentum balance, with

$$\nabla^2 = \frac{1}{r^2}\frac{\partial}{\partial r}\left(r^2\frac{\partial}{\partial r}\right). \tag{11.37}$$

Expanding the linear momentum balance equation, we have

$$-\frac{1}{\rho}\frac{\partial p}{\partial r} + \frac{\mu}{\rho}\left(\frac{\partial^2 v_r}{\partial r^2} + \frac{2}{r}\frac{\partial v_r}{\partial r} - \frac{2v_r}{r^2}\right) = \frac{\partial v_r}{\partial t} + v_r\frac{\partial v_r}{\partial r}. \tag{11.38}$$

If we now substitute the expression for v_r from mass balance into the term in the parentheses, we see that

$$6\frac{g(t)}{r^4} + \frac{2}{r}\left(-\frac{2g(t)}{r^3}\right) - 2\frac{g(t)}{r^4} = 0, \tag{11.39}$$

which is to say, linear momentum balance reduces to

$$-\frac{1}{\rho}\frac{\partial p}{\partial r} = \frac{\partial v_r}{\partial t} + v_r\frac{\partial v_r}{\partial r}. \tag{11.40}$$

It is interesting that this equation is independent of viscosity; indeed, if r is taken to be a streamline direction s, this is the same equation as the s-direction Euler equation (8.58) in the absence of gravity. This aneurysm–CSF problem is thus a special case wherein the same pressure and velocity fields satisfy both the Navier–Stokes and the Euler equations, as discussed in Observation 8.3 of Chap. 8. It is very important to recognize, however, that the viscosity of the fluid will still play a role through the stress boundary condition [Eq. (11.29)]. Before exploiting this, let us solve for the pressure field in the CSF. Although the fluid mechanicist would want to know the pressure at all values of r and t, the solid mechanicist only needs to know values at all $r = a$, which are felt by the solid (aneurysm). Hence, let us seek p at $r = a$ and thus integrate from a to ∞:

$$-\frac{1}{\rho}\int_a^\infty \frac{\partial p}{\partial r}dr = \int_a^\infty \frac{\partial}{\partial t}\left(\frac{g(t)}{r^2}\right)dr + \int_a^\infty v_r\frac{\partial v_r}{\partial r}dr, \tag{11.41}$$

or

$$-\frac{1}{\rho}p\Big|_a^\infty = \frac{dg(t)}{dt}\left(-\frac{1}{r}\Big|_a^\infty\right) + \frac{1}{2}v_r^2\Big|_a^\infty, \tag{11.42}$$

which yields

$$-\frac{1}{\rho}(p_\infty - p_a) = \frac{dg}{dt}\left(-\frac{1}{\infty} + \frac{1}{a}\right) + \frac{1}{2}\left(\frac{g^2}{\infty^4} - \frac{g^2}{a^4}\right), \tag{11.43}$$

or

$$p_a = \rho\left(\frac{dg}{dt}\frac{1}{a} - \frac{g^2}{2a^4}\right) + p_\infty. \tag{11.44}$$

Remembering that we are interested in the mechanics of an aneurysm within the head of a human, one might quickly ask the utility of integrating to infinity. In this case, infinity simply means far enough away from the aneurysm, which could be only centimeters (e.g., if $a = 1$ mm and "infinity" was merely taken to be 10 mm, then $1/1 - 1/10^2 = 0.99$ and $1/1 - 1/10^4 = 0.9999$, thus revealing that it is reasonable to neglect the terms $1/\infty^n$ in comparison to the $1/a^n$ terms). Note, too, that the deformed radius a and the integration function g are both functions of time; thus, the pressure exerted by the CSF on the aneurysm will likewise vary with time in general. Finally, the radial stress in the fluid is

$$\sigma_{rr} = -p + 2\mu\frac{\partial v_r}{\partial r} = -p + 2\mu\left(-\frac{2g(t)}{r^3}\right) \quad \forall r, t. \tag{11.45}$$

We are interested primarily in the stress at the wall of the aneurysm, where $r = a$. The normal stress in the fluid at this location thus becomes [using Eq. (11.44)]

$$\sigma_{rr}|_{r=a} = -p_a - 4\mu\frac{g(t)}{a^3} = \rho\left(\frac{g^2}{2a^4} - \frac{1}{a}\frac{dg}{dt}\right) - p_\infty - 4\mu\frac{g}{a^3}, \tag{11.46}$$

whereby we see that the viscosity of the CSF has indeed entered the problem through the stress boundary condition. At this point, note that we still have not found the arbitrary integration function $g(t)$, even though we have used a stress boundary condition at $r = a$ and the condition at infinity in the integration. When similar situations arose in Chaps. 3–5 for solids and Chaps. 9 and 10 for fluids, we sought additional conditions to generate the requisite number of equations for our unknowns. In particular, we often used kinematic conditions such as the continuity of displacement for two solids (e.g., bone and metal prosthesis in Chaps. 3 and 4) or velocities of two materials (e.g., a moving solid plate and underlying fluid in Couette flows in Chap. 9). To find $g(t)$, we can use a similar "matching condition" at $r = a$; that is, by the no-slip condition, we need to match the velocity of the aneurysm and that of the CSF at $r = a$. Given the displacement u_r in the r direction of a material point on the aneurysm, which

is the difference between where we are, $a(t)$, and where we were, A, the radial velocity of the aneurysmal wall is

$$\frac{du_r}{dt} = \frac{d}{dt}(a(t) - A) = \frac{da}{dt}, \tag{11.47}$$

where $a = \lambda A$. Thus, matching this velocity with $v_r(r = a, t)$ in the fluid, we have

$$\frac{du_r}{dt} = A\frac{d\lambda}{dt} = \frac{g(t)}{a^2} \equiv \frac{g(t)}{\lambda^2 A^2} \rightarrow g(t) = \lambda^2 A^3 \frac{d\lambda}{dt}. \tag{11.48}$$

It follows, therefore, that

$$\frac{dg}{dt} = A^3\left[\lambda^2\frac{d^2\lambda}{dt^2} + \frac{d\lambda}{dt}\left(2\lambda\frac{d\lambda}{dt}\right)\right]. \tag{11.49}$$

Hence, the outer stress boundary condition is

$$\begin{aligned}\sigma_{rr}|_{r=a} = &-\rho\left\{\frac{A^3}{\lambda A}\left[\lambda^2\frac{d^2\lambda}{dt^2} + 2\lambda\left(\frac{d\lambda}{dt}\right)^2\right] - \frac{\lambda^4 A^6}{2\lambda^4 A^4}\left(\frac{d\lambda}{dt}\right)^2\right\} - p_\infty \\ &- 4\mu\left[\frac{\lambda^2 A^3}{\lambda^3 A^3}\left(\frac{d\lambda}{dt}\right)\right],\end{aligned} \tag{11.50}$$

which can be simplified to

$$\begin{aligned}\sigma_{rr}|_{r=a} &= -\rho\left[A^2\lambda\frac{d^2\lambda}{dt^2} + 2A^2\left(\frac{d\lambda}{dt}\right)^2 - \frac{1}{2}A^2\left(\frac{d\lambda}{dt}\right)^2\right] - p_\infty - \frac{4\mu}{\lambda}\left(\frac{d\lambda}{dt}\right) \\ &= -\rho A^2\lambda\frac{d^2\lambda}{dt^2} - \frac{3}{2}\rho A^2\left(\frac{d\lambda}{dt}\right)^2 - \frac{4\mu}{\lambda}\left(\frac{d\lambda}{dt}\right) - p_\infty.\end{aligned} \tag{11.51}$$

The stress acting on the outer surface of the membrane in the positive r direction will be equal and opposite that in the fluid at $r = a$. Hence, the governing differential equation for the solid [Eq. (11.23), with $b \sim a$] can be written as

$$\left[-p_\infty - \rho A^2\lambda\frac{d^2\lambda}{dt^2} - \frac{3}{2}\rho A^2\left(\frac{d\lambda}{dt}\right)^2 - \frac{4\mu}{\lambda}\left(\frac{d\lambda}{dt}\right)\right] - [-P_i(t)] - \frac{2T}{\lambda A} = \frac{\rho_s HA}{\lambda^2}\frac{d^2\lambda}{dt^2}, \tag{11.52}$$

or

$$\left(\frac{\rho_s HA}{\lambda^2}+\rho A^2\lambda\right)\frac{d^2\lambda}{dt^2}+\frac{3}{2}\rho A^2\left(\frac{d\lambda}{dt}\right)^2+\frac{4\mu}{\lambda}\left(\frac{d\lambda}{dt}\right)+\frac{2T}{\lambda A}=P_i(t)-p_\infty, \quad (11.53)$$

where the time-varying blood pressure $P_i(t)$ is given by Eq. (11.27) and $T=T(\lambda)$ must be given by a constitutive equation for the aneurysm (recall Sect. 6.4 of Chap. 6). For example, for a Fung-type exponential behavior [cf. Eq. (6.41)], we have

$$T(\lambda)=c\Gamma e^{Q}\left(\lambda^2-1\right) \quad \text{with} \quad Q=\frac{1}{2}\Gamma\left(\lambda^2-1\right)^2, \quad (11.54)$$

where c and Γ are material parameters. Independent of the specific constitutive relation for the solid, however, we see how important the solid–fluid coupling is; the governing equation of motion for the dynamic response of the solid depends on the density ρ, viscosity μ, and far-field pressure p_∞ of the cerebrospinal fluid. This complex, nonlinear ordinary differential equation is solved numerically in Humphrey (2002) using a Runge–Kutta method. Figures 11.10 and 11.11 show one typical result, which suggests that this class of aneurysms is dynamically stable, contrary to the thoughts of many based on simplified linear analyses that neglected the nonlinear stress-stretch relation $T(\lambda)$ and the solid–fluid coupling. Although closed-form solutions are not available for Eq. (11.53), one can obtain analytical solutions for the stability of the aneurysm by linearizing the governing equation about multiple, different equilibrium positions—as noted in Observation 11.1, such linearizations can provide useful information on the nonlinear problem; that is, if one were to inflate the lesion to a particular equilibrium configuration and then perturb it slightly, one could ask whether the perturbed aneurysm (i.e., nonlinear system) would come back to its equilibrium configuration (i.e., be stable) or if it would move away from this configuration (i.e., be unstable). Recall that similar arguments were made in Chap. 5 in the fully linear analysis of the stability of Euler columns. Indeed, by performing a linearized stability analysis (see Humphrey 2002), it can be shown that it is the cerebrospinal fluid viscosity μ alone that renders the aneurysm dynamically stable in the nonlinear case given the assumptions invoked herein.

In summary, based on this analysis, it was concluded that at least one subclass of saccular aneurysms (nearly spherical) is unlikely to be dynamically unstable as postulated by some and supported by others based on simplified models. This illustrates the importance of modeling well the inherent complexities such as the nonlinear material behavior, the large deformations, and the solid–fluid coupling. Indeed, if one considers a viscoelastic, rather than purely elastic, behavior of the aneurysm, it can be shown that there is further evidence for

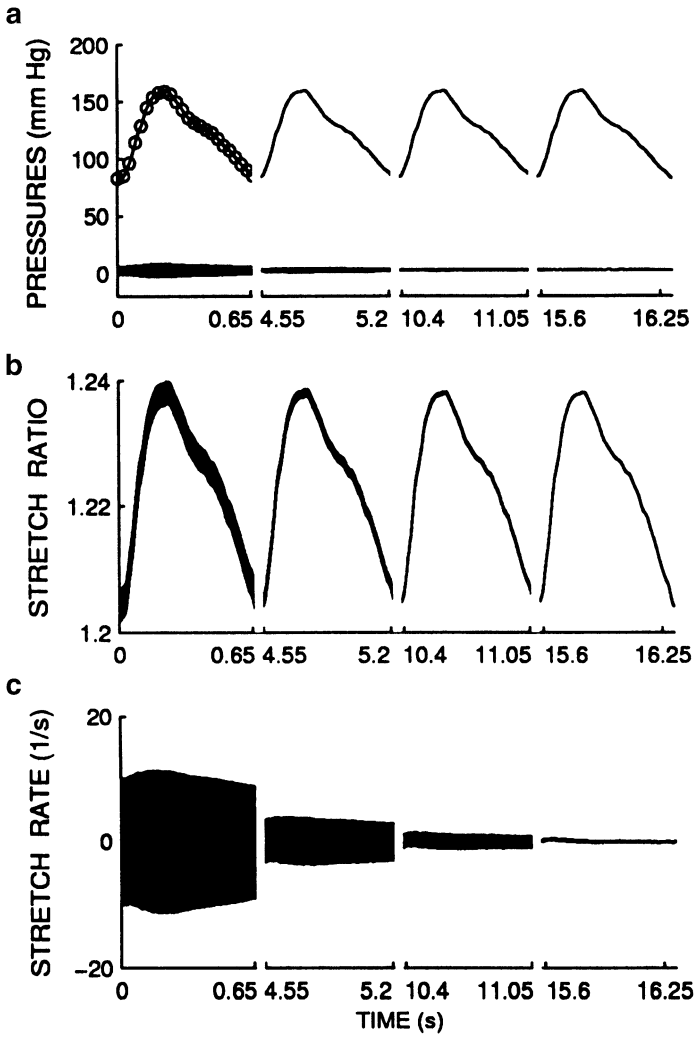

FIGURE 11.10 A representative result for the elastodynamics of an idealized spherical, isotropic saccular aneurysm. Panel *A* shows the internal forcing function $P_i(t)$, as both original human data (*open circles*) and their Fourier series representation (*solid lines*); the *bottom curve* shows the far-field pressure p_∞. Panels *B* and *C* show the associated time-varying stretch and stretch rate given an initial disturbance, which decreases quickly. With permission from Elsevier Science.

its dynamic stability. Rather than going into the details of the nonlinear viscoelasticity of solids, which is an important but advanced topic, we consider below an introduction to the linearized theory of viscoelasticity and some associated directions of needed research.

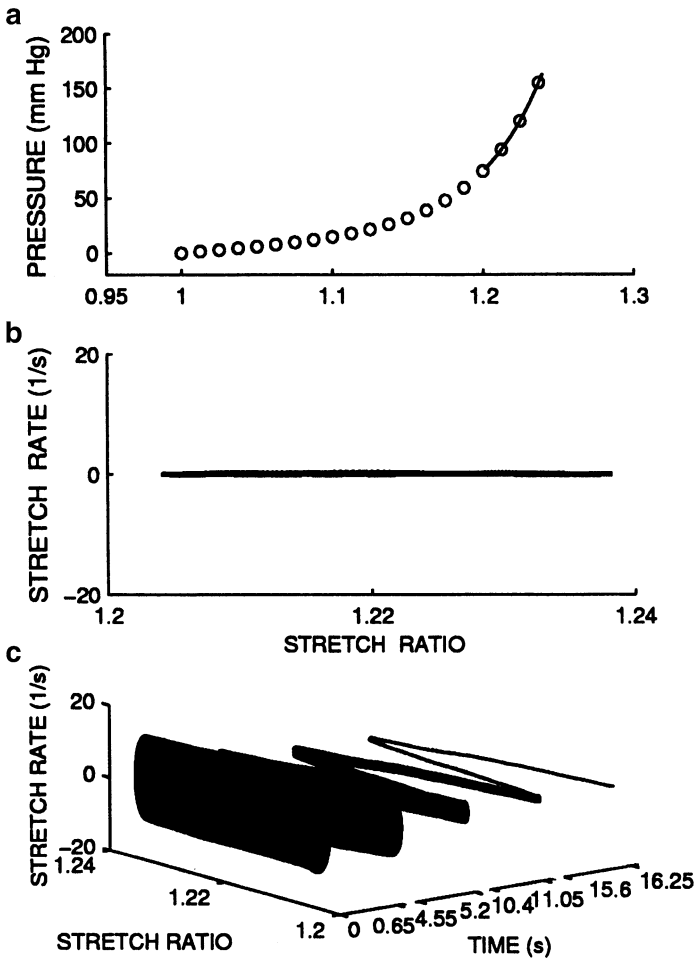

FIGURE 11.11 Further results associated with Fig. 11.10. Panel *b* shows the phase-plane in the case of no initial disturbance, that is, the periodic solution. Panel *c* shows the phase-time plot in the case of an initial disturbance, the effects of which are seen to decrease quickly such that the periodic solution is recovered (i.e., the periodic solution serves as a strong attractor), thus revealing that the system is dynamically stable. Finally, panel *a* shows the pressure-stretch behavior both for quasistatic loading (open circles) and for the dynamic case (solid line). Clearly, the inertial effects are small and the dynamics can be treated in terms of a series of equilibria. From Shah and Humphrey (1999), with permission from Elsevier Science.

Example 11.4 In Exercise 11.3, we ask that Eq. (11.53) be nondimensionalized to a simpler form. Here, we further neglect the fluid (nondimensional parameters $b=0$ and $m=0$) and assume a Fung-type behavior; thus our governing equation reduces to (Humphrey 2002)

$$\frac{1}{x^2}\ddot{x}+\frac{2}{x}\Gamma e^{Q}\left(x^2-1\right)=F(\tau),$$

where

$$Q=\frac{1}{2}\Gamma\left(x^2-1\right)^2.$$

Show that such a dynamic system is dynamically unstable in the small (i.e., in the absence of an external fluid and given small perturbations from an equilibrium position).

Solution: Let the nondimensional distending pressure at equilibrium be F_0 and the associated equilibrium stretch be $x=\alpha$. Moreover, let us consider a change in variables whereby

$$y_0\equiv x-\alpha \quad \text{and} \quad y_1\equiv dx/d\tau=\dot{x}.$$

Hence, our single second-order equation can be written in terms of two first-order equations, namely

$$\begin{aligned}\dot{y}_0&=\dot{x}=y_1,\\ \dot{y}_1=\ddot{x}&=\left[F_0-2\Gamma e^{Q}\left(x-\frac{1}{x}\right)\right]x^2,\end{aligned}$$

or in terms of the fixed point $x=\alpha$,

$$\begin{aligned}\dot{y}_0&=y_1,\\ \dot{y}_1&=\left[F_0-2\Gamma e^{Q}\left(y_0+\alpha-\frac{1}{y_0+\alpha}\right)\right](y_0+\alpha)^2,\end{aligned}$$

which we can write symbolically as

$$\begin{aligned}\dot{y}_0&=G(y_0,y_1;\alpha),\\ \dot{y}_1&=H(y_0,y_1;\alpha)\end{aligned}$$

where G and H are general functions. Expanding in a Taylor series about the fixed point $x = \alpha$, or $y_0 = 0$ and $y_1 = 0$, we have

$$\dot{y}_0 = G(0,0) + \left.\frac{\partial G}{\partial y_0}\right|_{(0,0)} (y_0 - 0) + \left.\frac{\partial G}{\partial y_1}\right|_{(0,0)} (y_1 - 0) + \ldots,$$
$$\dot{y}_1 = H(0,0) + \left.\frac{\partial H}{\partial y_0}\right|_{(0,0)} (y_0 - 0) + \left.\frac{\partial H}{\partial y_1}\right|_{(0,0)} (y_1 - 0) + \ldots,$$

where

$$G(0,0) = 0, \quad \frac{\partial G}{\partial y_0} = 0, \quad \frac{\partial G}{\partial y_1} = 1,$$
$$H(0,0) = 0, \quad \frac{\partial H}{\partial y_0} \neq 0, \quad \frac{\partial H}{\partial y_1} = 0.$$

Hence, our resulting system of linearized equations can be written in matrix form as

$$\begin{Bmatrix} \dot{y}_0 \\ \dot{y}_1 \end{Bmatrix} = \begin{bmatrix} 0 & 1 \\ \left.\frac{\partial H}{\partial y_0}\right|_{(0,0)} & 0 \end{bmatrix} \begin{Bmatrix} y_0 - 0 \\ y_1 - 0 \end{Bmatrix}.$$

As noted earlier, we know that dynamic stability in the small implies a dynamic stability of the associated nonlinear system. Such (asymptotic) stability requires that the trace of this matrix be negative and its determinant be positive. Note that the trace (i.e., the sum of the diagonal entries) is identically zero, however; thus, an elastic aneurysm cannot be asymptotically stable in the absence of a viscous CSF, which is consistent with results from the numerical solution. In this case, therefore, we see that knowing some results from the theory of systems of first-order, linear, ordinary differential equations provides significant insight without the need to perform complex numerical computations. Indeed, one should always pursue analytical results when possible.

11.4 Viscoelasticity: QLV and Beyond

Whereas the two previous sections address interactions between a "solid" and a "fluid," we now return our attention to the behavior of a single material. Recall from Fig. 1.4 of Chap. 1 that it is often convenient in continuum biomechanics to study separately the solidlike (biosolid mechanics) or fluidlike (biofluid

mechanics) behavior that is exhibited by a material under conditions of interest; indeed, courses and textbooks are often designed along these separate lines. Reflecting back on Chaps. 2–10, however, it should be evident that these divisions often are simply for convenience in particular classes of problems; they are not dictated by the physics per se. For example, our three primary governing differential equations—balance of mass, linear momentum, and energy—can be derived independent of the consideration of a solidlike or a fluidlike behavior. Likewise, our development of constitutive equations can follow a similar procedure (DEICE) regardless of the specific behavior, and it can result in similar relations (e.g., Hooke's law and the Navier–Poisson relation) whereby we relate the concept of stress to displacement gradients (strains) or velocity gradients (shear rates). Clearly, then, it should be very natural mathematically to consider together solidlike and fluidlike behaviors. Indeed, when we recognize that many materials—including glass over long time scales as well as the cytoplasm in a cell, the ligament in a joint, and even bone, to name but a few—simultaneously exhibit both a solidlike and a fluidlike behavior over conditions of interest, we should then pursue a more unified approach.

Traditionally, there have been two primary approaches to considering together solidlike and fluidlike behaviors. One is the so-called *theory of mixtures*, which traces its beginnings to Darcy and Fick in the mid-1800s, but received a more modern and rational treatment by Truesdell in 1957 [see the advanced text by Truesdell and Noll (1965, Section 130)]. Briefly, Truesdell postulated that one could model the behaviors of mixtures of multiple constituents, including solids and fluids, by requiring that (1) each constituent obey its own balance and constitutive relations and (2) the overall mixture obey the classical balance relations for mass, momentum, and energy. Such an approach requires that one identify an additional class of constitutive equations, however, which describe how the constituents exchange mass, momentum, and energy. For example, if a fluid flows through an otherwise stationary porous solid, the flow can induce a motion in the solid. Although we did not do so in Sect. 11.2, such interactions can be described directly by constitutive relations. V. Mow and colleagues were the first, in 1980, to apply the continuum theory of mixtures to biological tissues. They focused on the mechanical behavior of articular cartilage, which lines the contacting regions of bones in articulating joints and which consists primarily of a type II collagen, extensive proteoglycans, and mobile water. In fact, using the theory of mixtures, they show that the water carries much of the compressive load early in the gait cycle (Mow et al. 1990). Mixture theory continues to enable a much deeper understanding of cartilage mechanics than would have been possible if the solid mechanics had been studied alone. Since 1980, mixture theory has also been used to study the behavior of many different tissues and cells, and it remains as an important area of research, even in the emerging area of modeling growth and remodeling (Humphrey 2003a). Because of the inherent mathematical complexity, however, the theory of mixtures is beyond the scope of an introductory text.

The second general approach that has been used to address combined solidlike and fluidlike behaviors is the *theory of viscoelasticity*. As the name implies, its goal is to describe behaviors that include both an elastic and a viscous character. Developed in the mid-1800s by savants such as L. Boltzmann (1844–1906), J.C. Maxwell (1831–1879), and Lord Kelvin (1824–1907), this theory developed along two related but separate lines. Boltzmann advocated the use of heredity integrals to describe the history of the mechanical behavior; in contrast, Maxwell and Kelvin advocated the use of differential models to account for the rate effects. Both approaches are useful in biomechanics and both can be developed for linear or non-linear behaviors. Because the linear relations are much easier to address, however, we shall focus primarily on these.

11.4.1 Linearized Viscoelasticity

Bone and teeth are among the few tissues in the body that exhibit a linear relation between stress and strain over the range of physiologic strains. Although discussed thus far in terms of its solidlike behavior, bone exhibits viscoelastic characteristics. For example, the stress depends on the rate of deformation in addition to the amount of deformation (Fig. 11.12); in general, a viscoelastic response is stiffer at higher rates of deformation. Two other common characteristics that suggest a viscoelastic behavior are *creep* and *stress relaxation*. Creep is a time-dependent deformation under the action of a constant load (Fig. 11.13); stress relaxation is a time-dependent decrease in load at a constant deformation (Fig. 11.14). Toward a quantification of such behaviors, let us first consider a linearized, rate-type approach that may be used to describe the viscoelastic behavior of bone and other materials that exhibit a linear material behavior under small strains.

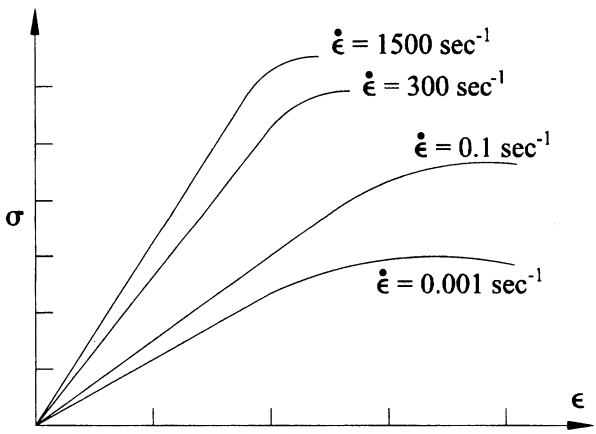

FIGURE 11.12 Strain-rate effects on the mechanical behavior of bone.

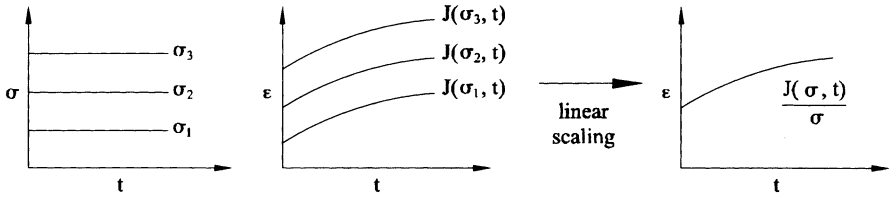

FIGURE 11.13 Characteristic responses to three different constant stresses during a creep test. By definition, *creep* is a continuing deformation (e.g., straining) in the presence of a constant force (or stress). In some cases, normalized creep responses reduce to a single characteristic curve.

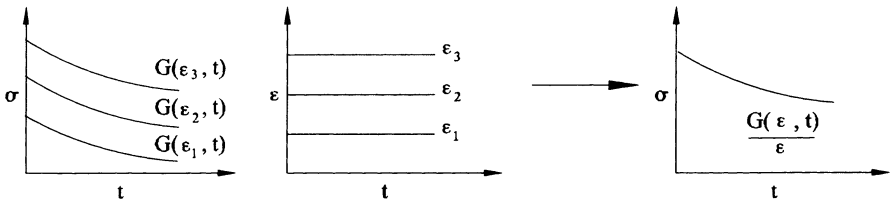

FIGURE 11.14 Similar to Fig. 11.13 except for *stress relaxation* (i.e., the continuing decrease in stress in the presence of a constant strain).

Maxwell Model

Maxwell, Kelvin, and others formulated their rate-type models in terms of 1-D mechanical analog models. Such models are only intended to simulate the macroscopic behavior; they are not designed to provide insight into the underlying molecular basis and they cannot be thought to be based on a general, rigorous mathematical foundation. Rather, analog models simply provide a means to motivate the forms of some constitutive relations.

The Maxwell model consists of a linear spring in series with a linear dashpot (Fig. 11.15). By linear, we mean that the force in the spring is related linearly to its extension and the force in the dashpot is related linearly to its rate of extension (Fig. 11.16). If we denote a scalar uniaxial force by f and the associated extension by δ (which is the current length x minus the original length x_o), this implies that $f_s = k\delta$ and $f_d = c\dot{\delta}$ where the subscripts s and d denote spring and dashpot, respectively, k is the stiffness of the spring, c is the viscosity of the dashpot, and the superimposed dot implies a time derivative. Remember that if a body is in equilibrium, then each of its parts are in equilibrium. Thus, a free-body diagram of the Maxwell element (Fig. 11.15) reveals that f_s and f_d each balance the total applied force f, whereas the total extension δ of the Maxwell element is the sum of the extensions of the spring

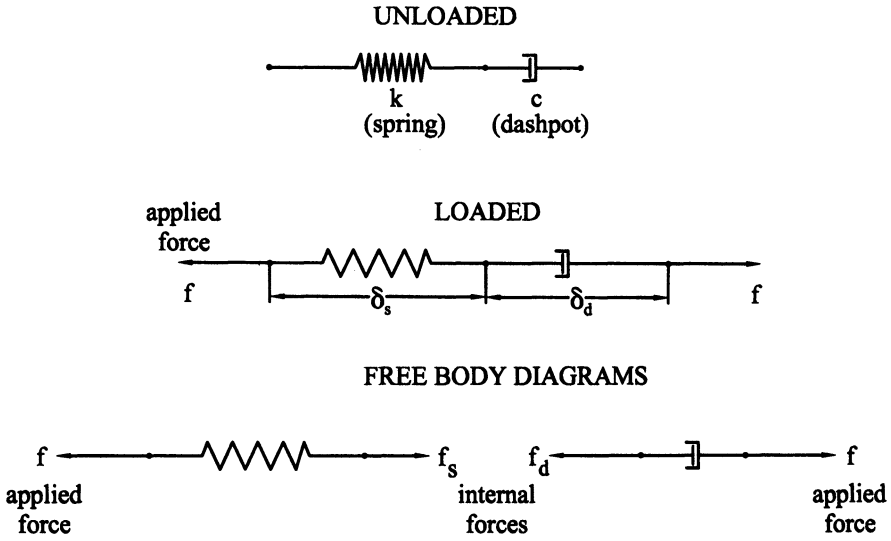

FIGURE 11.15 The Maxwell element consisting of a linear spring and dashpot in series in unloaded and loaded configurations. A free-body diagram reveals that the force (or stress) felt by the spring and the dashpot are the same.

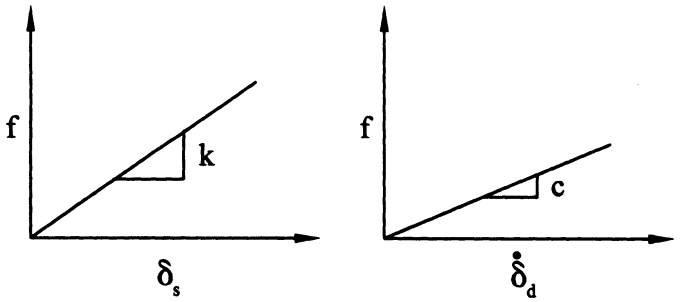

FIGURE 11.16 Mechanical behavior of a linear spring, with modulus k, and a linear dashpot, with viscosity c.

and the dashpot. Exploiting the latter observation, taking a time derivative, and using the appropriate constitutive relations, we obtain

$$\delta = \delta_s + \delta_d \rightarrow \dot{\delta} = \dot{\delta}_s + \dot{\delta}_d = \frac{\dot{f}}{k} + \frac{f}{c}. \tag{11.55}$$

Because this is an analog model, it is assumed that an associated 1-D relation in terms of the Cauchy stress σ and linearized strain ε is

$$\dot{\varepsilon} = \frac{\dot{\sigma}}{E} + \frac{\sigma}{\mu}, \tag{11.56}$$

where $\dot{\varepsilon}$ and $\dot{\sigma}$ are the strain rate and stress rate, respectively, E is the Young's modulus, and μ is the viscosity. This is the fundamental constitutive relation for the 1-D Maxwell model of linear viscoelasticity.

Consistent with Fig. 11.14, a stress relaxation test can be defined by $\varepsilon = 0$ for $t < 0$ and $\varepsilon = \varepsilon_0$, a constant, for $t \geq 0$. Hence, $\dot{\varepsilon} = 0$ for all $t \geq 0$ and Eq. (11.56) reduces to

$$0 = \frac{\dot{\sigma}}{E} + \frac{\sigma}{\mu} \rightarrow \dot{\sigma} + \frac{E\sigma}{\mu} = 0 \quad \forall t \geq 0. \tag{11.57}$$

This homogeneous, first-order differential equation admits an exponential solution of the form

$$\sigma(t) = c_1 e^{-Et/\mu}, \tag{11.58}$$

which can be verified (do it) by direct substitution. The value of the constant c_1 can be determined by letting $\sigma(t = 0) = \sigma_0$, where the assumption of an instantaneous (elastic) response requires that $\sigma_0 = E\varepsilon_0$. Hence, $c_1 = \sigma_0$ and the stress relaxation of a Maxwell model is given by either

$$\sigma(t) = \sigma_0 e^{-Et/\mu} \quad \text{or} \quad \sigma(t) = \sigma_0 e^{-t/t_R}, \tag{11.59}$$

where $t_R \equiv \mu/E$ is the so-called *relaxation time*. The larger the value of t_R, either via a large μ or a small E, the slower the relaxation. Clearly, at $t = 0$, $\sigma(0) = E\varepsilon_0$, the instantaneous elastic response, whereas for $t \rightarrow \infty$, $\sigma(t) \rightarrow 0$ with an exponential decay. Because this model relaxes to zero stress, it is sometimes called a Maxwell fluid. It is, nonetheless, a model that accounts for combined solidlike and fluidlike behaviors in general.

In contrast, the creep test is defined by $\sigma = 0$ for $t < 0$ and $\sigma \equiv \sigma_0$, a constant, for all $t \geq 0$. Hence, $\dot{\sigma} = 0$ for $t \geq 0$ and $\dot{\varepsilon} = \sigma_0/\mu$, which appears to describe a Newtonian fluidlike behavior consistent with the above. With regard to the associated creep, however, we see that

$$\int \frac{d\varepsilon}{dt} dt = \int \frac{\sigma_0}{\mu} dt \rightarrow \varepsilon(t) = \frac{\sigma_0}{\mu} t + c_1, \tag{11.60}$$

where $\varepsilon = \varepsilon_0$ at $t = 0$, the instantaneous response. Hence, with $\varepsilon_0 = \sigma_0/E$, we have $c_1 = \varepsilon_0$ and

$$\varepsilon(t) = \frac{\sigma_0}{\mu} t + \frac{\sigma_0}{E}. \tag{11.61}$$

This suggests that the creep (i.e., lengthening over time) is linear in t. Experimental observations reveal that most "biosolids" that exhibit a viscoelastic character do not relax to zero stress and they do not creep linearly in time. There is clearly a need to consider other models.

Kelvin–Voigt Model

This mechanical analog model is defined by a linearly elastic spring and a dashpot in parallel, not in series (Fig. 11.17). A free-body diagram reveals that $f = f_s + f_d$ and $\delta = \delta_s = \delta_d$. Hence,

$$f = k_s\delta + c\dot{\delta}, \tag{11.62}$$

which suggests a 1-D analog model of the form

$$\sigma = E\varepsilon + \mu\dot{\varepsilon} \rightarrow \dot{\varepsilon} + \frac{E}{\mu}\varepsilon = \frac{\sigma}{\mu}. \tag{11.63}$$

In contrast to the Maxwell model, therefore, a stress relaxation test (i.e., $\varepsilon = 0$ for $t < 0$ and $\varepsilon = \varepsilon_0$ for $t > 0$, with $\dot{\varepsilon} = 0$ for $t > 0$) leads to the simple relation that

$$\sigma(t) = E\varepsilon_0 \quad \forall t > 0, \tag{11.64}$$

which states that there is no relaxation for $t > 0$ (see Exercise 11.13 for behavior at $t = 0$). For creep, with $\sigma = \sigma_0$ for $t \geq 0$, we have a simple non-homogenous, first-order differential equation for $\varepsilon(t)$, namely

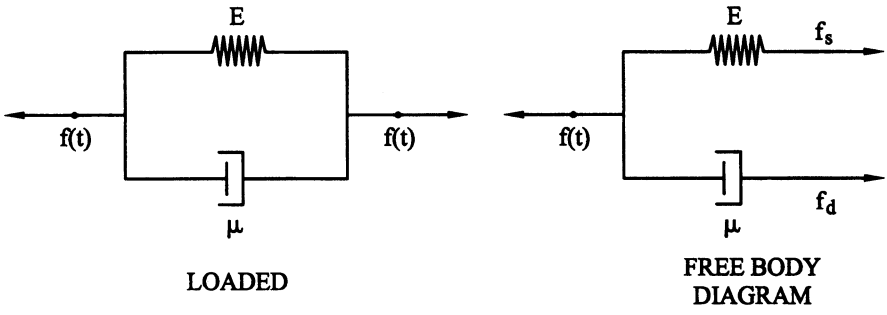

FIGURE 11.17 The Kelvin–Voigt element consisting of a linear spring and dashpot in parallel.

$$\dot{\varepsilon} + \frac{E}{\mu}\varepsilon = \frac{\sigma_0}{\mu}. \tag{11.65}$$

The homogenous solution is thus exponential:

$$\dot{\varepsilon} + \frac{E}{\mu}\varepsilon = 0 \rightarrow \varepsilon_h(t) = c_1 e^{c_2 t} \tag{11.66}$$

whereby $c_2 = -E/\mu$. The particular solution can be assumed to be constant, $\varepsilon_p(t) = c_3$ whereby $c_3 \equiv \sigma_0/E$. Hence, our solution is

$$\varepsilon(t) = c_1 e^{-Et/\mu} + \frac{\sigma_0}{E}. \tag{11.67}$$

Finally, the condition at $t = 0$ that $\varepsilon(0) = 0$ requires $c_1 = -\sigma_0/E$, thus yielding our creep response:

$$\varepsilon(t) = \frac{\sigma_0}{E}\left(1 - e^{-Et/\mu}\right) = \frac{\sigma_0}{E}\left(1 - e^{-t/t_c}\right), \tag{11.68}$$

where $t_c = \mu/E$ is called the *retardation time*. Note that at $t = 0$, $\varepsilon(0) = 0$, whereas at $t \rightarrow \infty$, $\varepsilon \rightarrow \sigma_0/E$. Hence, the creep is nonlinear, but bounded.

In summary, neither the Maxwell nor the Kelvin–Voigt model reflects commonly observed behavior in tissues. In particular, the linear and unbounded creep predicted by the Maxwell model is unrealistic, so, too, is the lack of relaxation for the Kelvin–Voigt model. Given that the instantaneous elasticity and relaxation of the Maxwell model and the nonlinear, bounded creep of the Kelvin–Voigt model are realistic, at least qualitatively; thus, one might consider combining these models with each other or perhaps combining them with other spring or dashpot elements. We shall consider such possibilities next. First, however, it proves useful to define two functions: $G(t)$, the *relaxation function* (during a stress relaxation test), and $J(t)$, the *creep function* (during a creep test). In particular, we let

$$G(t) = \frac{\sigma(t)}{\varepsilon_0}, \quad J(t) = \frac{\varepsilon(t)}{\sigma_0}; \tag{11.69}$$

hence, for the Maxwell model,

$$G(t) = Ee^{-Et/\mu}, \quad J(t) = \frac{1}{\mu}t + \frac{1}{E}, \tag{11.70}$$

whereas for the Kelvin–Voigt model,

$$G(t) = E, \quad J(t) = \frac{1}{E}\left(1 - e^{-Et/\mu}\right). \tag{11.71}$$

These will prove useful below.

Standard Viscoelastic Solid

It can be shown that combining a linear spring in parallel with a Maxwell element or combining a spring in series with a Kelvin–Voigt element (Fig. 11.18) yields the same differential equation. For example, if E_0 is the stiffness of the spring that is added in parallel to a Maxwell element, the governing equation can be shown to be

$$\dot{\sigma} + \frac{E}{\mu}\sigma = \frac{EE_0}{\mu}\varepsilon + (E + E_0)\dot{\varepsilon}. \tag{11.72}$$

For stress relaxation, it can be shown that (Wineman and Rajagopal 2000),

$$\sigma(t) = \varepsilon_0\left(E_0 + Ee^{-Et/\mu}\right), \tag{11.73}$$

and for creep,

$$\varepsilon(t) = \sigma_0\left[\frac{1}{E_0} + \left(\frac{1}{E_0 + E} - \frac{1}{E_0}\right)\exp\left(\frac{-E_0E}{\mu(E + E_0)}t\right)\right]. \tag{11.74}$$

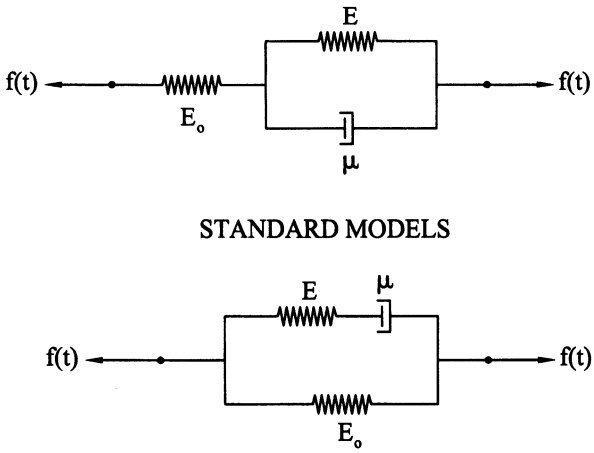

FIGURE 11.18 The standard element: either a spring in series with a Kelvin–Voigt element or a spring in parallel to a Maxwell element.

Consequently, the relaxation and creep functions can be written as

$$G(t) = E_0 + (E + E_0 - E_0)e^{-t/t_R} \equiv G_\infty + (G_0 - G_\infty)e^{-t/t_R} \tag{11.75}$$

where $G_\infty \equiv E_0$ and $G_0 \equiv E + E_0$, and

$$J(t) = J_\infty + (J_0 - J_\infty)e^{-t/t_c}, \tag{11.76}$$

where $J_0 = 1/G_0$ and $J_\infty = 1/G_\infty$ and the retardation time $t_c = G_0 t_R / G_\infty$. Figures 11.19 and 11.20 compare the associated characteristic responses. The Standard model is thus the simplest mechanical analog model that gives physically realistic predictions for viscoelastic "solids," including instantaneous elasticity, a nonlinear but bounded creep, and a stress relaxation that tends to a nonzero equilibrium stress.

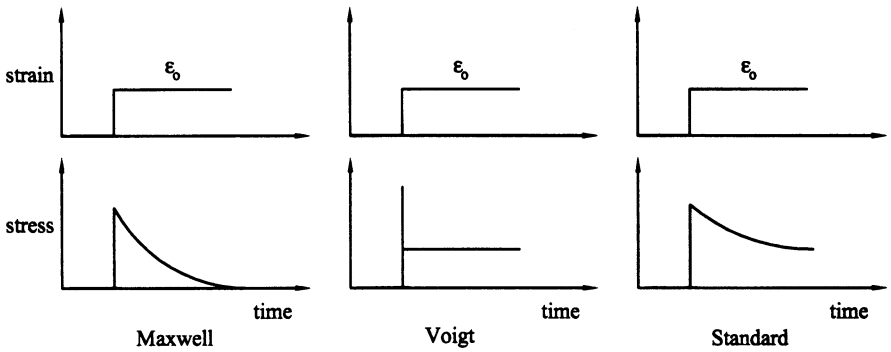

FIGURE 11.19 Characteristic stress relaxation responses of the Maxwell, Kelvin–Voigt, and Standard element consistent with the derivations in the text.

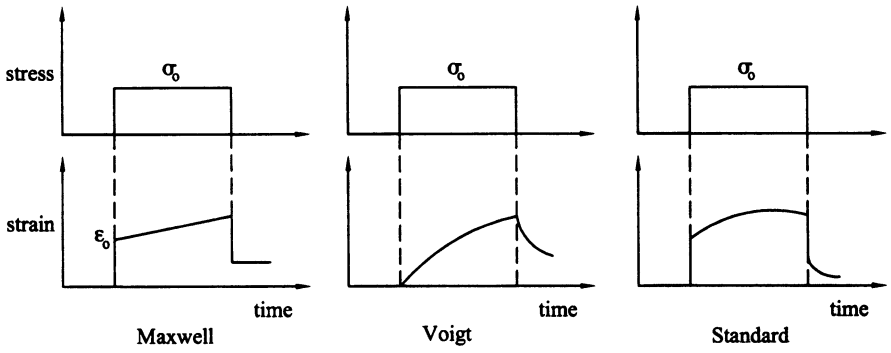

FIGURE 11.20 Similar to Fig. 11.19 except for creep.

Example 11.5 Derive the governing equation for a three-element viscoelastic fluid defined by a dashpot (viscosity μ_0) in series with a Kelvin–Voigt element (viscosity μ_v, and modulus E_v).

Solution: Let the total stress and strain of the three-element model (draw it, including free body diagrams) be σ and ε, respectively. By equilibrium, the stress in the single dashpot σ_0 must balance the stress in the Kelvin–Voigt element σ_v, and both must equal σ. Note, therefore, that

$$\sigma_0 = \mu_0 \dot{\varepsilon}_0, \quad \sigma_v = E_v \varepsilon_v + \mu_v \dot{\varepsilon}_v.$$

Moreover, the total strain $\varepsilon = \varepsilon_0 + \varepsilon_v$, where the strains in the spring and dashpot of the Kelvin–Voigt element are the same. Hence, with $\sigma = \sigma_v$ and $\varepsilon_v = \varepsilon - \varepsilon_0$, we have

$$\sigma = E_v(\varepsilon - \varepsilon_0) + \mu_v(\dot{\varepsilon} - \dot{\varepsilon}_0),$$

whereby

$$\dot{\sigma} = E_v(\dot{\varepsilon} - \dot{\varepsilon}_0) + \mu_v(\ddot{\varepsilon} - \ddot{\varepsilon}_0).$$

Now, note that $\dot{\varepsilon}_0 = \sigma_0/\mu_0$ and thus $\ddot{\varepsilon}_0 = \dot{\sigma}_0/\mu_0 \equiv \dot{\sigma}/\mu_0$. Hence, we have

$$\dot{\sigma} = E_v\left(\dot{\varepsilon} - \frac{\sigma_0}{\mu_0}\right) + \mu_v\left(\ddot{\varepsilon} - \frac{\dot{\sigma}_0}{\mu_0}\right)$$

or

$$\dot{\sigma}\left(1 + \frac{\mu_0}{\mu_0}\right) + \sigma\left(\frac{E_v}{\mu_0}\right) = E_v\dot{\varepsilon} + \mu_v\ddot{\varepsilon}$$

or

$$\sigma + \dot{\sigma}\left(\frac{\mu_0 + \mu_v}{E_v}\right) = \mu_0\dot{\varepsilon} + \frac{\mu_v\mu_0}{E_v}\ddot{\varepsilon}.$$

Compare this to the three-element (standard) viscoelastic solid.

Boltzmann Model

As noted earlier, Boltzmann advocated a different approach to modeling viscoelastic behavior; he focused on heredity integrals to account for the history of the response, and, in particular, the creep and stress relaxation.

For example, standard linear heredity integrals are

$$\sigma(t) = \int_{-\infty}^{t} G(t-s)\frac{d\varepsilon}{ds}ds \tag{11.77}$$

and

$$\varepsilon(t) = \int_{-\infty}^{t} J(t-s)\frac{d\sigma}{ds}ds. \tag{11.78}$$

It proves useful to evaluate these integrals over two intervals: from $-\infty$ to 0 and from 0 to time t, where

$$\int_{-\infty}^{t}(\ )ds = \int_{-\infty}^{0}(\ )ds + \int_{0}^{t}(\ )ds. \tag{11.79}$$

Hence, our relations for stress and strain histories can be shown to be

$$\sigma(t) = \varepsilon(0)G(t) + \int_{0}^{t} G(t-s)\frac{d\varepsilon}{ds}ds \tag{11.80}$$

and

$$\varepsilon(t) = \sigma(0)J(t) + \int_{0}^{t} J(t-s)\frac{d\sigma}{ds}ds. \tag{11.81}$$

In many cases, we have zero stress and strain up to and at the time $t = 0$; hence, these equations simplify further. We shall consider such cases below.

In contrast to the aforementioned stress relaxation and creep tests, which are very useful in evaluating viscoelastic responses, let us consider here a class of *sinusoidal straining* tests. Such tests are particularly useful for evaluating "short-time" responses in contrast to the "long-time" responses in creep and relaxation tests. Hence, consider a periodic strain history of the form

$$\varepsilon(t) = \varepsilon_A \sin \omega t \tag{11.82}$$

where ω is the fundamental (circular) frequency of the test (with $2\pi f = \omega$) and ε_A is the amplitude of the small strain. In order to use Eq. (11.80), with $\varepsilon(0) = 0$,

it proves convenient to consider a change of variables: let $t - s = \tau$ whereby $s = t - \tau$ at any fixed time t. Hence,

$$\frac{d}{ds}(\ ) = \frac{d}{d\tau}(\ )\frac{d\tau}{ds} = -\frac{d}{d\tau}(\ ), \quad ds = -d\tau. \tag{11.83}$$

Equation (11.80), with $\varepsilon(0) = 0$ and $\tau \in [0, \infty)$, can thus be written as

$$\sigma(t) = \int_0^\infty G(\tau)\frac{d\varepsilon(t-\tau)}{d\tau}d\tau = \int_0^\infty G(\tau)\dot{\varepsilon}(t-\tau)d\tau. \tag{11.84}$$

Given that $\dot{\varepsilon}(t) = \varepsilon_A \omega \cos \omega t$, we have

$$\sigma(t) = \int_0^\infty G(\tau)\varepsilon_A \omega \cos \omega(t-\tau)d\tau, \tag{11.85}$$

or by using the standard trigonometric identity that $\cos(\alpha \pm \beta) = \cos\alpha \cos \beta \mp \sin\alpha \sin\beta$, we have

$$\sigma(t) = \int_0^\infty G(\tau)\varepsilon_A \omega(\cos \omega t \cos \omega\tau + \sin \omega t \sin \omega\tau)d\tau, \tag{11.86}$$

or

$$\begin{aligned}\sigma(t) = (\varepsilon_A \cos \omega t)\omega \int_0^\infty G(\tau)\cos \omega\tau d\tau \\ + (\varepsilon_A \sin \omega t)\omega \int_0^\infty G(\tau)\sin \omega\tau d\tau.\end{aligned} \tag{11.87}$$

If we now denote

$$\begin{aligned}G_1(\omega) &\equiv \omega \int_0^\infty G(\tau)\sin(\omega\tau)d\tau, \\ G_2(\omega) &\equiv \omega \int_0^\infty G(\tau)\cos(\omega\tau)d\tau,\end{aligned} \tag{11.88}$$

then

$$\sigma(t) = \varepsilon_A[G_1(\omega)\sin \omega t + G_2(\omega)\cos \omega t], \tag{11.89}$$

where $G_1(\omega)$ and $G_2(\omega)$ are called the *storage modulus* and the *loss modulus*, respectively.

At this juncture, it is instructive to note that if subjected to a strain history of the form $\varepsilon(t) = \varepsilon_A \sin \omega t$, then we expect a viscoelastic material to respond out of phase, such as $\sigma(t) = \sigma_A \sin(\omega t + \phi)$. Conversely, if the response is purely elastic, we expect $\phi = 0$, whereas if the response is purely viscous, we expect $\phi = \pi/2$. Computation of the value of ϕ in general can thus be revealing. Note, therefore, that given this expression for $\sigma(t)$, we have

$$\sigma(t) = \sigma_A(\sin \omega t \cos \phi + \cos \omega t \sin \phi). \tag{11.90}$$

Comparison of Eqs. (11.89) and (11.90) thus reveals that

$$\begin{aligned} \varepsilon_A G_1(\omega) &= \sigma_A \cos \phi \rightarrow G_1(\omega) = \frac{\sigma_A}{\varepsilon_A} \cos \phi, \\ \varepsilon_A G_2(\omega) &= \sigma_A \sin \phi \rightarrow G_2(\omega) = \frac{\sigma_A}{\varepsilon_A} \sin \phi, \\ \tan \phi &= G_2(\omega)/G_1(\omega). \end{aligned} \tag{11.91}$$

Finally, note that it can be useful to use a complex variable ($z^* = Ax + iy$, with $i = \sqrt{-1}$) representation for these sines and cosines. It can be shown that if $\varepsilon^*(t) = \varepsilon_A e^{i\omega t}$ and $\sigma^*(t) = \sigma_A e^{i\omega(t+\phi)}$, then a *complex modulus*

$$G^* = \frac{\sigma^*}{\varepsilon^*} = G_1 + iG_2. \tag{11.92}$$

In this case, it is evident that G_1 is the ratio of that part of the stress that is in-phase with the strain to the strain itself, whereas G_2 is the ratio of that part of the stress that is $\pi/2$ out-of-phase with the strain to the strain itself.

For a purely elastic (i.e., Hookean) response, therefore, $G_1 = 1$ and $G_2 = 0$, with $\phi = 0$, and for a purely viscous (i.e., Newtonian) response, $G_1 = 0$ and $G_2 = 1$, with $\phi = \pi/2$. Computation of these moduli can thereby enable one to assess the "degree" of the viscoelastic response [i.e., its deviation from a purely elastic or a purely viscous response (cf. Fig. 11.21)].

Example 11.6 Demonstrate why G_2 is called the loss modulus.

Solution: Consider the energy dissipated during a simple cycle of loading:

$$\xi = \int \sigma d\varepsilon \equiv \int_0^{2\pi/\omega} \sigma \frac{d\varepsilon}{dt} dt.$$

If we let, consistent with Exercise 11.16,

$$\varepsilon(t) = \varepsilon_A \sin \omega t, \quad \sigma(t) = \sigma_A \sin(\omega t + \phi),$$

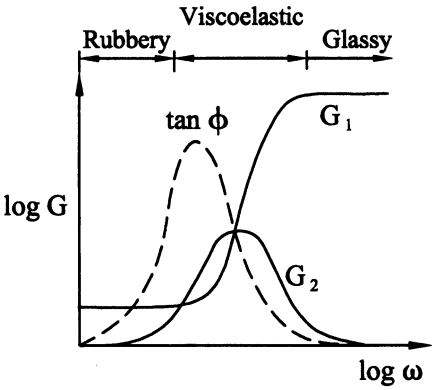

FIGURE 11.21 Characteristic complex moduli for viscoelastic behaviors in rubbery and glassy regimes.

then

$$\xi = \int_0^{2\pi/\omega} \sigma_A(\sin\omega t\cos\phi + \cos\omega t\sin\phi)\varepsilon_A\omega\cos\omega t\,dt$$
$$= (\sigma_A\cos\phi)\varepsilon_A\omega\int_0^{2\pi/\omega}\sin\omega t\cos\omega t\,dt + (\sigma_A\sin\phi)\varepsilon_A\omega\int_0^{2\pi/\omega}\cos^2\omega t\,dt,$$

which, from integral tables, yields

$$\xi = \left(\frac{\sigma_A\cos\phi}{\varepsilon_A}\right)\varepsilon_A^2\omega\left(\frac{1}{2\omega}\sin^2\omega t\Big|_0^{2\pi/\omega}\right)$$
$$+ \left(\frac{\sigma_A\sin\phi}{\varepsilon_A}\right)\varepsilon_A^2\omega\left(\frac{1}{2}t + \frac{1}{4\omega}\sin 2\omega t\Big|_0^{2\pi/\omega}\right)$$

or, from Exercise 11.16,

$$\xi = G_1\varepsilon_A^2\left(\frac{1}{2}\right)(0) + G_2\varepsilon_A^2\omega\left[\left(\frac{1}{2}\right)\left(\frac{2\pi}{\omega}\right)\right] = \pi G_2\varepsilon_A^2,$$

thereby revealing that the dissipation (i.e., loss) in this linear model is given entirely by the "loss modulus" G_2.

In summary, this has been but a brief introduction to a few aspects of *linear* viscoelasticity. For more on this topic, the reader is encouraged to consult Ferry (1980) or Wineman and Rajagopal (2000).

11.4.2 Quasilinear Viscoelasticity

Because of the nonlinear material behavior exhibited by most soft tissues, linearized relations for viscoelasticity do not apply. In an attempt to account for the nonlinear "elastic" behavior while preserving the mathematical machinery of linear viscoelasticity, Fung proposed a so-called *quasilinear theory of viscoelasticity*, often referred to as QLV.

Briefly, following Boltzmann's approach, Fung suggested that, in one dimension, one should consider the following relationship for the first Piola–Kirchhoff stress Σ_{11} and stretch λ (Fung 1990):

$$\Sigma_{11}(t) = \int_{-\infty}^{t} G(t-\tau) \frac{\partial \Sigma_{11}^{e}}{\partial \lambda} \frac{d\lambda}{d\tau} d\tau, \tag{11.93}$$

where G is a reduced relaxation function, with $G(0) = 1$, $\Sigma_{11}^{e}(\lambda)$ is a nonlinearly elastic response function (in terms of the first Piola–Kirchhoff stress), and λ is an axial stretch ratio. Fung noted that it is common to express the relaxation function in terms of a finite sum of exponential decay functions. Noting problems common to such approaches, including finding $G(\infty)$, Fung further noted that the observed relative insensitivity of the hysteresis during cyclic loading of many soft tissues suggests the need for a continuous relaxation spectrum. The literature reveals many subsequent applications of Fung's QLV theory. We will leave it as an exercise to explore such applications, however.

11.4.3 Need for Nonlinear Theories

This subsection could simply be entitled "Beyond QLV." Despite the success of QLV in fitting data from various experiments, numerous investigators have shown that QLV is not sufficiently general to describe many of the complicated behaviors exhibited by soft tissues, including a strain-dependent relaxation and fundamentally different short-term and long-term viscoelastic responses. Building upon the many fundamental advances in nonlinear viscoelasticity since World War II [by G. Green, R. Rivlin, A.C. Pipkin, and B. Bernstein et al., among others; see Ferry (1980)], various approaches have been proposed. These include the single integral finite strain model of Johnson et al. (1996), the combined differential–integral model of Pioletti and Rakotomanana (2000), the generalized elastic-Maxwell model of Holzapfel and Gasser (2001) and Holzapfel et al. (2002), and the modified superposition model of Provenzano et al. (2002), to name but a few. Like mixture theory, however, nonlinear viscoelasticity is not an introductory topic; thus, the reader is simply encouraged to seek advanced courses on this topic. When doing so, remember that science is but relative truth; thus, each theory and approach is limited. Noting

any restrictions or limitations, particularly those in small strain theories, is of paramount importance as we seek to use biomedical engineering design and analysis to improve health care.

11.5 Lubrication of Articulating Joints

11.5.1 Biological Motivation

Human diarthroidal joints can function well for seven or more decades despite the relatively high loads and at times low speeds of relative motion that they experience. For example, tissue stresses can reach 18 MPa in the knee during just normal walking. Recall from Chap. 7 that synovial fluid serves as a tremendous lubricant that reduces wear of cartilage in articulating joints such as the knee and hip; the coefficient of friction in joints is an amazing 0.003–0.03, much less than values attained by man-made lubricants. The mechanics of lubrication is a well-developed area of study in mechanical engineering, called *tribology*, and one may be tempted to apply results from tribology directly to the analysis of knee or hip mechanics. Indeed, as early as the 1930s, it was suggested that the efficiency of healthy diarthroidal joints could be explained via the theory of hydrodynamic lubrication; that is, it was thought that loads are transferred between articulating surfaces via a thin, pressurized layer of fluid lubricant. Let us briefly consider a simple example of such a theory of lubrication.

11.5.2 Hydrodynamic Lubrication

Consider the "hydrodynamic slider bearing" shown in Fig. 11.22. Let us assume that the fluid behavior is Newtonian and that the flow is incompressible, steady, and laminar. It would seem reasonable, therefore, to assume the velocity field of the fluid to be of the form $\boldsymbol{v} = v_x(x, y)\hat{\boldsymbol{i}} + v_y(x, y)\hat{\boldsymbol{j}}$ in the absence of gravity. If we assume further that the Reynolds' number is small (Re < 1), then viscous

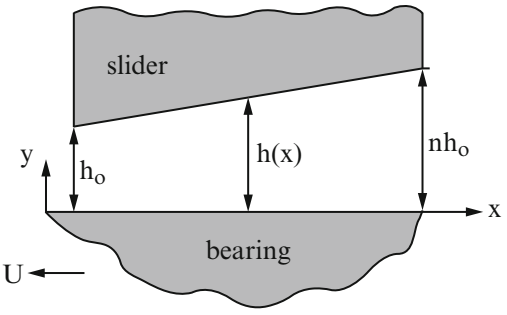

FIGURE 11.22 The slider bearing, which supports a compressive load W due to hydrodynamic lubrication. Let the length of the slider be L.

effects dominate inertial effects. Moreover, if we assume that the gap distance $h(x) \ll L$, then the x-direction momentum equation is most important and changes in v_x with respect to y may be considered to be less than those with respect to x. Hence, the Navier–Stokes equation in x [Eq. (8.34)] reduces to

$$\frac{dp}{dx} = \mu \frac{d^2 v_x}{dy^2} \tag{11.94}$$

and our problem is similar to that in Chap. 9 for flow between parallel flat plates. In particular, our general solution is

$$v_x(y) = \frac{1}{\mu}\left(\frac{dp}{dx}\right)\frac{y^2}{2} + c_1 y + c_2. \tag{11.95}$$

Now, for boundary conditions. Here, let us consider the simplified case of a step-slider (Fig. 11.23). Hence, we have

$$v_x(0) = -U, \quad v_x(h) = 0, \quad 0 \le x < L - bL, \tag{11.96}$$

$$v_x(0) = -U, \quad v_x(nh) = 0, \quad L - bL < x \le L, \tag{11.97}$$

and Eq. (11.95) becomes

$$v_x(y) = \frac{1}{2\mu}\left(\frac{dp}{dx}\right)(y^2 - nhy) + U\left(\frac{y}{nh} - 1\right) \tag{11.98}$$

for $n = 1$ or n, in general. Hence, the volumetric flow rate is

$$Q = \int_0^w \int_0^h v_x(y)\,dy\,dz = -\frac{n^3 h^3 w}{12\mu}\left(\frac{dp}{dx}\right) - \frac{Unhw}{2} \tag{11.99}$$

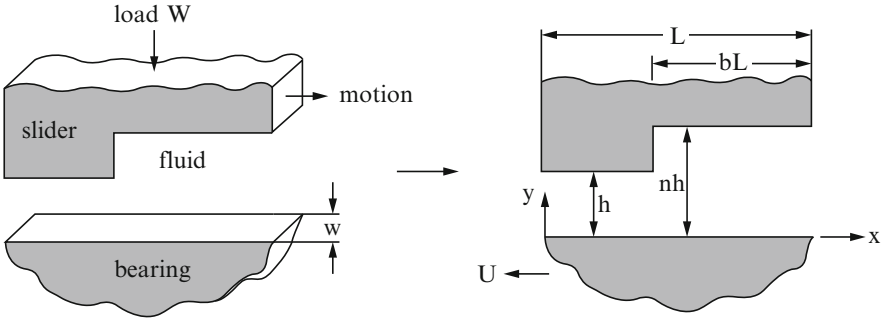

FIGURE 11.23 A step-slider bearing showing important loads and dimensions.

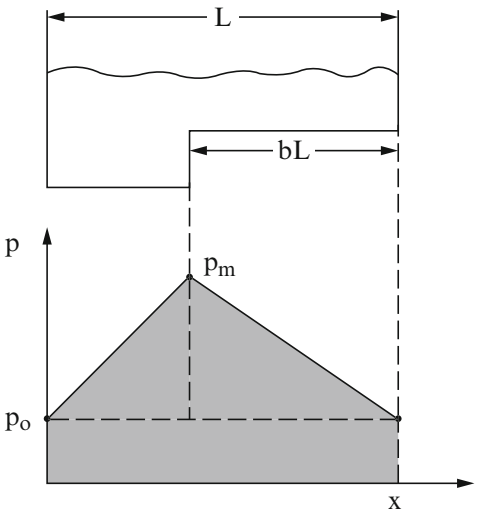

FIGURE 11.24 Computed pressure distribution for the step-slider bearing shown in Fig. 11.23.

for $n=1$ or n. Because Q must be a constant

$$Q_1 = -\frac{h^3 w}{12\mu}\left(\frac{dp}{dx}\right)_1 - \frac{Uhw}{2} = -\frac{n^3 h^3 w}{12\mu}\left(\frac{dp}{dx}\right)_2 - \frac{Unhw}{2} = Q_2, \qquad (11.100)$$

which is to say, (dp/dx) must be a constant over $0 \le x < L - bL$ and also over $L - bL < x \le L$; that is, p must be linear in each of these two domains (Fig. 11.24). We let

$$\left(\frac{dp}{dx}\right)_1 = \frac{p_m - p_o}{L(1-b)}, \quad \left(\frac{dp}{dx}\right)_2 = \frac{p_o - p_m}{bL} \qquad (11.101)$$

where p_m is the value of the pressure at $x = L(1-b)$ and p_o is the uniform pressure outside the slider on both the right and the left ends. Let us now solve for $p_m - p_o$ using the constraint that $Q_1 = Q_2$. We find that

$$-\frac{h^3 w}{12\mu}\left(\frac{p_m - p_o}{L(1-b)}\right) - \frac{Uhw}{2} = -\frac{n^3 h^3 w}{12\mu}\left(\frac{p_o - p_m}{bL}\right) - \frac{Unhw}{2}, \qquad (11.102)$$

or

$$(p_m - p_o)\left(\frac{h^3 w}{12\mu L}\right)\left(\frac{1}{1-b} + \frac{n^3}{b}\right) = \frac{Uhw}{2}(n-1). \qquad (11.103)$$

Hence,

$$p_m - p_o = \frac{6\mu ULwb}{h^2}\left(\frac{(n-1)(1-b)}{b+n^3(1-b)}\right). \tag{11.104}$$

The associated total vertical load W that the slider can support is

$$\begin{aligned} W &= p_o(LW) + \frac{1}{2}(L-bL)(p_m - p_o)w + \frac{1}{2}(bL)(p_m - p_o)w \\ &= p_o(LW) + \frac{1}{2}Lw(p_m - p_o) = W_{static} + W_{dyn}. \end{aligned} \tag{11.105}$$

Defining the dynamic load-carrying capability as W_{dyn}, we can define a nondimensional *load coefficient* C_w as

$$C_w = W_{dyn}\left(\frac{h^2}{U\mu L^2 w^2}\right) = \frac{3b(n-1)(1-b)}{b+n^3(1-b)}. \tag{11.106}$$

This formula can be used by the design engineer to determine preferred values of b and n to maximize C_w given any other design constraints. Note, however, that if $n=1$ or $b=0$, the step disappears and the dynamic load-carrying capacity is lost. This is the case in parallel plates, or the so-called Couette flow. Finally, note that a frictional drag coefficient C_f can also be defined as the total drag force F_D divided by the total vertical load-bearing capacity W. It can be shown that

$$C_f = \frac{F_D}{W} = \frac{h(n-1)}{L} + \frac{h[n(1-b)+b][b+n^3(1-b)]}{3Lbn(n-1)(1-b)}. \tag{11.107}$$

Obviously, we seek to minimize C_f while maximizing C_w.

Whereas a step-slider (Fig. 11.23) allows us to begin to appreciate some aspects of hydrodynamic lubrication, such a sharp geometric discontinuity is clearly unrealistic in the case of an articulating joint, even a prosthetic one. Hence, one would be more likely to consider the *inclined slider* (Fig. 11.22). The solution of this problem is similar but more complex because $h=h(x)$. It can be shown, however, that if $h(x)$ changes linearly, then

$$p(x) - p_o = \frac{\mu ULw}{h_o^2}\left(\frac{6(n-1)(1-x/L)(x/L)}{(n+1)[n+(n-1)(x/L)]^2}\right), \tag{11.108}$$

where $h(x)=h_o[1+(n-1)(x/L)]$. For $L \gg h_o$, one finds a parabolic distribution of pressure with load and frictional load coefficients

$$C_w = \frac{6}{(n-1)^2}\left(\ln n - \frac{2(n-1)}{n+1}\right), \tag{11.109}$$

$$C_f = \frac{h_o(n-1)}{L}\left(\frac{\ln n}{6\ln n - 12(n-1)/n+1} + \frac{1}{2}\right). \tag{11.110}$$

Despite the simplicity of this and similar analyses, mechanical engineers can describe well and thus design many efficient bearings. Yet, this conventional hydrodynamic lubrication theory reveals that a continuous, highspeed operation (i.e., speed U) is needed between the two opposing solid surfaces to maintain a sufficient pressure and thus thickness of the lubricant. High-speed relative motion is not a characteristic of the articulating joint, however; thus, the mechanics of diarthroidal joints is more complex. We are reminded, therefore, that biomechanics is not just mechanics applied to biology; many times, it must include the development or extension of mechanics to solve a biologically important problem.

In the 1960s, attention in orthopedic biomechanics turned toward coupled theories that included both the flow of the lubricant and the deformation of the solid load-bearing surfaces. Such *elastohydrodynamic* theories were based on the assumption that compression of the cartilage caused it to spread out and thereby increase the surface area over which the load was applied. It was argued that lower stresses would induce less wear. Nevertheless, such theories could not explain many empirical findings and they still suggested the need for relatively high speeds of relative motion between the load-bearing surfaces; there remained a need for more appropriate analyses. One such idea was called the *squeeze-film* theory. Recall from Fig. 7.14 that synovial fluid exhibits a non-Newtonian character. Basically, it was suggested that a hydrostatic pressure would be generated in the synovial fluid when the two load-bearing solid surfaces were brought closer together and that this was due in part to the high apparent viscosity of the synovial fluid at low shear rates and at long times of applied stress. Nevertheless, it seemed that an important aspect of the biophysics was still being neglected.

From the 1960s to the 1980s, others began to consider the "porous" nature of the cartilage. One suggestion was that when the cartilage was loaded, interstitial fluid would be exuded and this fluid would aid in the lubrication. Such theories were referred to as *weeping lubrication*, which allowed for a load-dependent, self-pressurizing mechanism. Conversely, others suggested a so-called *boosted lubrication* whereby the water portion of the synovial fluid was forced into the cartilage, thus leaving a higher-viscosity, strongly non-Newtonian solution consisting primarily of hyaluronan in the joint space. Consideration of such scenarios (i.e., cases of fluids diffusing within solids) led to the widespread use of the aforementioned theory of mixtures in cartilage mechanics, which we discuss briefly in the following section.

Observation 11.2. Glycosaminoglycans, often simply referred to as GAGs, consist of linear chains of repeating disaccharide units; they are highly negatively charged and thereby tend to sequester water and contribute directly to the compressive, rather than tensile, stiffness of a soft tissue. The four primary classes of GAGs are hyaluronan, chondroitin sulfate/dermatan sulfate, heparan sulfate, and keratan sulfate. Hyaluronan is unique in that it does not associate directly with a protein core. It expands significantly when hydrated and occupies large volumes of the extracellular space, thus allowing it to resist compressive loads and to facilitate cell migration; it is particularly abundant in morphogenesis and early wound healing. When GAGs associate with a protein core, the composite molecules are called proteoglycans (PGs). In addition to serving as space-filling, negatively charged gels within the extracellular matrix, PGs also control the activity of many cytokines, chemokines, and proteases.

In normal heart valves, for example, the PGs biglycan and decorin tend to exist in regions of cyclic tension whereas hyaluronan and the PG versican tend to aggregate in regions of cyclic compression. The former is consistent with biglycan and decorin contributing to collagen fibrillogenesis whereas the latter is consistent with the ability of versican to bind hyaluronan and form large multi-molecular hydrophilic complexes that support compressive loads. In particular, the fixed negative charges associated with many of the GAGs/PGs perturb the local balance of cations within the extracellular matrix and induce so-called *Donnan swelling pressures*. Briefly, the so-called Donnan effect explains how mechanical equilibrium and electroneutrality can both be maintained while gradients or jumps exist in mobile ions (e.g., Na^+ in an aqueous solution) due to a region of the system containing fixed molecules that are charged (e.g., negative charges due to SO_3^- or COO^- groups within GAGs). These ionic gradients or jumps, in turn, alter the regional distribution of interstitial water and, as in the case of GAGs, cause a localized swelling pressure within the region containing the fixed charges. See Cowin and Doty (2007) for more details on modeling the Donnan effect.

11.5.3 Need for a Mixture Theory

As noted earlier, in 1980, Mow and colleagues proposed the use of the theory of mixtures to account for the combined fluid and solidlike behavior exhibited by articular cartilage. Here is a very brief synopsis, which comes from Mow et al. (1990). Cartilage consists of ~50–73 % type II collagen, 15–30 % proteoglycan, and ~5 % chondrocytes by dry weight; by wet weight, cartilage consists of 58–78 % water. These constituents are organized in a highly complex, nonhomogeneous fashion (Fig. 11.25). In particular, the collagen is oriented differently in the superficial, middle, and deep "zones," and the collagen and

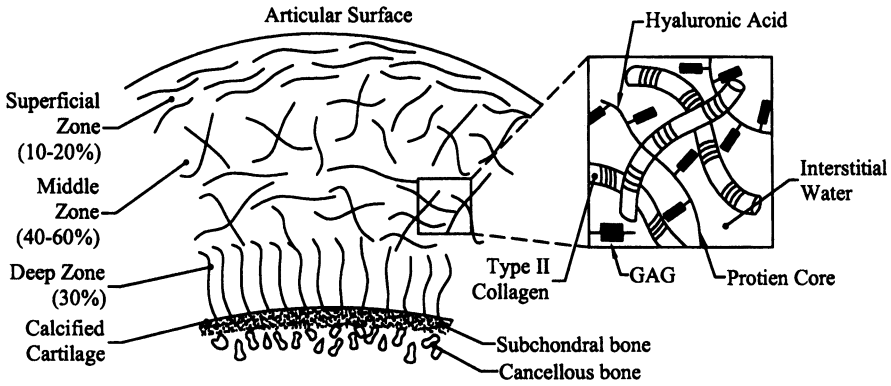

FIGURE 11.25 Schema of articular cartilage showing the strong nonhomogeneity in composition and its solid–fluid mixture constitution, which is dominated by water, proteoglycans, and type II collagen. Recall, for example, that tendons, ligaments, and bones (other structurally significant members of an articulating joint) consist largely of type I collagen, not type II. Thus, cartilage possesses a unique structure consistent with its unique function. Hyaluronic acid is also called hyaluronan.

proteoglycans form a complex composite microstructure. The collagen is packed more densely in the superficial and deep zones; thus, most of the proteoglycans are located in the middle zone. The proteoglycans contribute significantly to the compressive and swelling properties. Mow and colleagues idealized this structure as a porous matrix (collagen + proteoglycans, or solid phase) that is swollen with water (a liquid phase), both bound and unbound. In other words, there was no attempt to model directly the complex interactions (physical entanglements, electrostatic bonds, and excluded volume) between proteoglycans and collagen; attention was focused on the volume-averaged mean composite behavior of the solid portion of the tissue. Of particular importance, however, is the ability of applied loads to cause the interstitial fluid to redistribute within the cartilage or to flow out of or into the cartilage. One of the key parameters describing such a behavior is thus the permeability of the tissue, which was measured via confined compression tests wherein a sample was placed above a rigid porous filter and loaded from above. The permeability was found to decrease nonlinearly with applied compressive strain, typical values being on the order of $(0.5 - 2) \times 10^{-15}$ m^4/Ns. Other important material parameters included the moduli for the solid (Young's modulus and Poisson's ratio because of the assumption of a linear elastic behavior by the solid portion) and diffusive drag coefficient. The latter was a measure of the ease that the fluid could diffuse through the solid and thus was inversely related to the permeability. Indeed, rather than modeling the viscosity of the interstitial fluid directly, the diffusive drag coefficient was used to capture this dissipative characteristic. Viscoelastic effects can thus be modeled, in part,

through solid–fluid interactions even though more recent studies suggest the need to account for the intrinsic viscoelastic behavior of the "solid." Although the basic formulation is straightforward, solution of even simple initial and boundary value problems is nontrivial; in particular, it is very difficult to identify appropriate boundary conditions between a non-Newtonian (synovial) fluid and a solid–fluid mixture (cartilage). Thus, the reader is referred to advanced texts. The take-home message here is that, again, we see the importance of modeling coupled phenomena in soft tissue biomechanics.

Observation 11.3. In this chapter, we have discussed but a few of the many biological and clinical problems wherein one must understand both the biosolid and the biofluid mechanics, including many cases of direct fluid-solid interactions. As the reader might imagine, there are many more such examples.

Albeit perhaps not typically thought of within the context of biomechanics, it is becoming increasingly recognized that the study of cancer and cancerous cells requires attention to the mechanics. Simply put, cancer is characterized by uncontrolled cell division as well as the properties of invasion and metastasis in the formation of tumors. Cancerous tumors typically exhibit different material properties than those of the surrounding healthy tissue, which can be exploited in diagnosis (e.g., detection via ultrasound, or elastography). Because of their heightened growth, cancerous tumors require increased oxygen and thus angiogenic development of a vascular network, which can be considered a therapeutic target (i.e., attenuation of the angiogenic growth). Hence, it is easy to appreciate roles of both biosolid and biofluid tissue mechanics.

In addition, however, the excellent review by Suresh (2007) highlights the importance of understanding cell mechanics from the perspective of cellular migration, cytoadherence, neoplastic transformation, and so forth. For example, Suresh asks "How could the information on structure—mechanical property—biological function—disease state relationships guide the development of novel tools for disease diagnostics, prophylactics and therapeutics, as well as drug efficacy assays?" He then proceeds to review via a flowchart how structure-property-function relations are related within the context of complex diseases such as cancer, to review the biology of cancer cells while focusing on important biomechanical and chemomechanical factors such as angiogenesis, cellular invasion into blood vessels and lymph, and transport to other locations where the cells actively extravasate (i.e., migrate across the vascular wall) and metastasize. He also reviews the importance of quantifying mechanical properties of cells (via nine different experimental approaches, including AFM and optical tweezers) and understanding the mechanics of the cytoskeleton, particularly the

actin, intermediate filaments, and microtubules. As noted throughout, therefore, solid and fluid mechanics at multiple scales is fundamental to understanding and treating diverse diseases, even cancer.

11.6 Thermomechanics, Electromechanics, and Chemomechanics

Continuum mechanics rests upon three fundamental balance relations that yield our equaitons of motion: mass, linear momentum, and energy. With the exception of the development of the pipe-flow equation in Chap. 10, we have focused on the balance of mass and linear momentum. One reason for this is that the energy equation is particularly important in nonisothermal problems, but the body tends to regulate its temperature within a narrow range ($37 \pm 2\ ^\circ\text{C}$). Nevertheless, there are many cases wherein *biothermomechanics* is important (Humphrey 2003b). In particular, advances in laser, microwave, radio-frequency, and other technologies has motivated the widespread use of supraphysiologic temperatures to treat a wide variety of diseases and injuries. Examples include the treatment of joint laxity (e.g., severe sprains), visual problems (e.g., LASIK surgery and secondary cataracts), skin defects (e.g., port wine stains and melanomas), chronic pain, cardiovascular disorders (e.g., atrial fibrillation and obstructive atherosclerotic lesions), gynecological disorders (e.g., endometriosis), prostate problems (e.g., benign prostatic hyperplasia as well as malignancies), and so on. Such treatments denature proteins and kill cells thereby affecting the biomechanical properties of the treated tissues as well as the associated mechanobiology; the latter being particularly important with regard to the post-treatment healing response. For example, if a thermal treatment alters the biomechanical properties, and perhaps the geometry, of a tissue or organ, then different stresses will result due to normal in vivo loads. An altered state of stress, in turn, will alter cellular activity via mechanotransduction mechanisms, including possible changes in cell migration, proliferation, apoptosis, and production and removal of the matrix. Hence, not only is the response to the initial (thermal) injury important, so too is the biomechanics. There is, therefore, a pressing need to study coupled thermomechanical problems. For example, soft tissues will often change their extensibility and hydration in response to thermal damage. Hence, there is a need to address the fluidlike, solidlike, and thermal behaviors together. Again, however, biothermomechanics is inherently complex and nonlinear, and detailed design and analysis are beyond the scope of an introductory text.

Nonetheless, to illustrate the importance of combining thermal and mechanical analyses, let us consider a simple example. Recall from Chaps. 2–4 that metallic implants are commonly used in joint replacements, particularly in the hip and knee. Moreover, although there are multiple ways of securing such

devices within the host tissue, one commonly used method is to "cement" the device in place. Bone cements, such as poly(methyl-methacrylate) or PMMA, are injected into the space between the bone and prosthesis and allowed to polymerize (cf. Fig. 4.10). This process involves an exothermic reaction, which is to say, one that gives off "heat." A concern, therefore, is whether the transfer of heat from the curing cement to the bone might thermally damage the bone cells, which, in turn, would compromise the bone-implant interface. As a first approximation of this problem, one could consider a structure consisting of three concentric, circular layers: the inner metallic prosthesis, the layer of PMMA, and the outer layer of cortical bone. The bioheat transfer problem could be assumed to be axisymmetric; hence, from Eq. (A10.12) of Chap. 10, the basic heat transfer equation could be written in terms of temperature T as

$$\rho c_v \frac{\partial T}{\partial t} = k\left[\frac{1}{r}\frac{\partial}{\partial r}\left(r\frac{\partial T}{\partial r}\right)\right] + \rho q_s \tag{11.111}$$

for each layer, where c_v and k are the specific heat and thermal conductivity, respectively, of each material. Recall, too, that q_s is a so-called volumetric heat source or sink. One of the important realizations in biomechanics is that flowing blood is capable of convecting away significant amounts of heat. In 1948, H. Pennes suggested that one could model this convective loss through the q_s term (i.e., as a heat sink). Determination of a reasonable constitutive relation for q_s thus requires that we couple the analyses of heat transfer and blood flow. Similarly, recall from Eqs. (2.69) of Chap. 2 that the strains in a solid depend on both the state of stress and the temperature. Hence, changes in temperature within the three materials (prosthesis, cement, and bone) will change their states of stress and strain. Clearly, the solid mechanics should be coupled with that of the analysis of the heat transfer. Without going into mathematical detail, therefore, we see that even in a simple example, solid mechanics, fluid mechanics, and heat transfer should be addressed in coupled fashion to design well a common clinical procedure.

With the exception of a brief discussion in Chap. 6, we have not addressed the mechanics of muscle. There are a number of reasons for this, not the least of which is that our understanding of muscle mechanics remains inadequate. Nevertheless, it should be clear that the biomechanics of athletic performance, rehabilitation, cardiac health, the vasculature, and many other areas depends primarily on an understanding of muscle mechanics. In particular, heart disease remains a leading cause of morbidity and mortality, and biomechanics has great potential to impact treatment in many ways—from the design of artificial hearts and assist devices to understanding thermal treatments such as atrial ablation. Cardiac function (i.e., the filling and ejecting of blood from the heart to the rest of the body) depends on a strong *electromechanical coupling*; that is, the propagation of electrical signals dictates the order of contraction of cardiac muscle fibers, which, in turn, dictates cardiac output. There is, therefore, a

pressing need to couple our study of the electrical activity and mechanical performance of the heart. Being an advanced topic, however, we merely refer the reader to the literature, including the excellent books by Glass et al. (1991) and Panfilov and Holden (1997).

Finally, although not emphasized earlier, it should be clear from Chaps. 2–10 that the mechanics is coupled strongly with the biochemistry in many cases. For example, with regard to biological growth and remodeling, A. Turing recognized in the 1950s that one must not only quantify the effects of stress and strain on tissue response (e.g., Wolff's law of bone remodeling), one must also account for the rate at which various molecules (e.g., morphogens) are produced by the cells and the diffusion of such molecules throughout the tissue. Cellular production and molecular diffusion are each affected directly by the mechanics (e.g., pressure gradients); thus, such studies must address the *chemomechanical* coupling. Indeed, recent data suggest that even the contractility of smooth muscle cells in early hypertension may be governed, in part, by a pressure-induced increase in the conversion of G-actin to F-actin in the cytoplasm (i.e., a pressure-induced chemical reaction called polymerization).

Similarly, we mentioned earlier that there is a need to couple mechanics and thermodynamics in studies of the use of heat to treat disease and injury. One of the most commonly used equations in biothermomechanics is that of S. Arrhenius, which states that the rate k of a chemical reaction (e.g., denaturation of a protein) depends on the temperature given two material parameters, the activation energy E_a and gas constant R, namely

$$k(T) = A \exp\left(-\frac{E_a}{RT}\right). \tag{11.112}$$

Recent data suggest, however, that the rate of thermal denaturation also depends on the state of stress in the tissue: A higher stress tends to delay the denaturation at a given temperature. It should be noted, therefore, that the parameter A in Arrhenius's relation can be shown to be related to an activation entropy. It is well known that tissue elasticity is primarily entropic (i.e., determined primarily by load-induced changes in the conformations of molecules), not energetic (as in metals). It is clear, therefore, that the chemical reactions responsible for the thermal denaturation of a protein or the thermal death of a cell depend on the thermodynamics and the solid mechanics. See Humphrey (2003b) for more detail on these and related issues in biothermomechanics.

In summary, most real-world problems necessitate that we address coupled problems—solid–fluid, thermomechanical, electromechanical, chemomechanical, and, indeed, thermomechanochemical and so on. Toward this end, we should first learn well the basics in each discipline, knowing that important contributions will come from appropriate synthesis. Interdisciplinary and multidisciplinary research teams thus hold great promise and should be pursued vigorously.

Chapter Summary

Whereas Chaps. 2–6 focused on the mechanics of materials that exhibit solidlike behaviors and Chaps. 7–10 focused on materials that exhibit fluidlike behaviors, there are many cases wherein either there exist *fluid-solid-interactions* or the material simultaneously exhibits both solidlike and fluidlike characteristics. Like Chap. 6, the goal of this chapter was simply to introduce new topics having increased complexity—the interested reader is encouraged to seek more advanced books on both nonlinear material behavior and coupled phenomena.

Section 11.2 is particularly important for it illustrates the use of the *Buckingham Pi* theorem (cf. Sect. 10.5) in designing and interpreting a revealing experiment, in this case for the diffusion of a viscous fluid through a finitely deformed permeable membrane. Figure 11.5 shows, for example, that permeability varies nonlinearly with finite deformation.

In contrast, Sect. 11.3 illustrates an *elastodynamic* solution of a problem of importance in neurosurgery, which reveals the importance of capturing relevant solid-fluid interactions and using nonlinear rather than linear elasticity to describe the response of this soft tissue. Indeed, note that this same problem was addressed before by others who neglected both the surrounding cerebral spinal fluid and the nonlinear stress-stretch behavior of the wall, which not unexpectedly resulted in wrong conclusions regarding the possible stability of the lesion.

Combined solidlike and fluidlike behaviors classified as *viscoelastic* are especially important in biomechanics under particular conditions of interest. Section 11.4 briefly introduces this topic, but the interested reader is referred to other textbooks devoted to this subject. Similar to many of these text books, Sect. 11.4.1 focuses on a 1-D linearized theory, which applies to limited situations in biomechanics but helps one to build intuition nonetheless. In particular, like the Bernoulli equation for an ideal fluid, linearized viscoelasticity has been misused frequently in the literature because of the neglect of limitations of the theory. Such misuse has appeared at both the cell and tissue levels.

In addition, to the need to appreciate nonlinear viscoelasticity, the reader is encouraged to study concepts of poroelasticity and mixture theory as applied to biomechanics. See for example the book by Cowin and Doty (2007) and references therein. Indeed, we conclude Chap. 11 with an illustrative example of hydrodynamics of lubrication, a topic that is typically aligned closely to the use of elastohydrodynamics and mixture theory to understand the mechanics of joints in orthopedic research. The reader is referred to Mow and Hayes (1991) for more on this and related topics.

Appendix 11: Wave Equations

Recall that we studied the steady flow of a Newtonian fluid within a rigid circular cylinder in Sect. 9.2. Notwithstanding the unsteadiness of flow in actual arteries and airways, results for steady flows are often used to estimate the mean wall shear stress within arteries and airways as well as in the more appropriate applications of flows in veins, gravity-fed IV tubes, and so forth. Inasmuch as the unsteadiness can be important, we also considered a special case of pulsatile flow within a rigid circular cylinder in Sect. 9.5, which provided more insight into potential effects of pulsatility on wall shear stress. Yet, as noted eloquently by Zamir (2000), pulsatile flows differ fundamentally within rigid tubes versus either elastic or viscoelastic tubes (e.g., arteries, airways, and so forth). No matter how small the distensibility of the tube, flow propagates within a distensible tube as a wave having a finite wave speed. Hence, in the presence of any downstream material or geometric discontinuity (e.g., a bifurcation or a branch), the wave(s) can reflect, which can lead to forward and backward traveling waves that add either constructively or destructively. In the case of constructive interference, for example, a local systolic blood pressure due to a forward traveling wave can be augmented by a backward traveling wave, which thereby increases the local pulse pressure. Of course, an increased pulse pressure in the ascending aorta can increase the work-load on the heart whereas an increased pulse pressure within any segment of the arterial tree can also be a strong mechanobiological stimulus for cells within the wall of the artery.

In contrast, waves do not exist in a rigid tube. The so-called wave speed is infinite in a rigid tube (recall the Moens-Korteweg equation in Observation 7.2), which means that the pressure and flow are transmitted instantaneously along the length of the tube, hence resulting in an overall bulk motion. There is, therefore, strong motivation to study unsteady flows in distensible tubes, that is, fluid-solid-interactions. Indeed, as we also noted in Observation 7.2, "pulse wave velocity" (PWV) within large arteries is now recognized as an important indicator or initiator of diverse cardiovascular diseases and it merits increased scientific consideration. Although the complexities of analytical or computational solutions of wave motion within a distensible vasculature are beyond the scope of an introductory textbook, let us note some basics with regard to traveling waves.

A number of equations in mathematical physics exhibit common features and can be classified as elliptic, parabolic, or hyperbolic (partial) differential equations. They are,

$$\begin{aligned} &\textit{Elliptic} && 0 = \nabla^2\phi, \\ &\textit{Parabolic} && \frac{\partial\phi}{\partial t} = \alpha^2\nabla^2\phi, \\ &\textit{Hyperbolic} && \frac{\partial^2\phi}{\partial t^2} = c^2\nabla^2\phi, \end{aligned} \tag{A.11.1}$$

where α and c are parameters, $\nabla^2 \equiv \frac{\partial^2}{\partial x^2} + \frac{\partial^2}{\partial y^2} + \frac{\partial^2}{\partial z^2}$ in three spatial dimensions (3-D) in Cartesian coordinates, and t is time. These equations are known, respectively, as the Laplace equation, the diffusion equation, and the wave equation; general methods of solution can be found in textbooks on partial differential equations or applied mathematics.

Let us consider briefly the wave equation in one spatial dimension (1-D), namely

$$\frac{\partial^2 \phi}{\partial t^2} = c^2 \frac{\partial^2 \phi}{\partial x^2}, \tag{A.11.2}$$

where c is a constant and we seek solutions of the form $\phi = \phi(x,t)$, where x is the spatial coordinate location and t is time. It was recognized by D'Alembert that functions of the form $\phi = \phi(x - ct)$ and $\phi = \phi(x + ct)$ satisfy this linear partial differential equation, hence these solutions can be superimposed to yield the general solution, $\phi = \phi(x - ct) + \phi(x + ct)$, which suggests that a wave could begin at $x = 0$ and travel simultaneously in both the positive and negative direction at speed c. That these functions satisfy the wave equation can be appreciated easily by noting that, if $\phi = \hat{\phi}(u)$, with $u = x - ct$, then

$$\begin{aligned} \frac{\partial \phi}{\partial t} &= \frac{\partial \hat{\phi}}{\partial u}\frac{\partial u}{\partial t} = \frac{\partial \hat{\phi}}{\partial u}(-c) \text{ and } \frac{\partial^2 \phi}{\partial t^2} = \frac{\partial^2 \hat{\phi}}{\partial u^2}(-c)(-c) \\ \frac{\partial \phi}{\partial x} &= \frac{\partial \hat{\phi}}{\partial u}\frac{\partial u}{\partial x} = \frac{\partial \hat{\phi}}{\partial u}(1) \text{ and } \frac{\partial^2 \phi}{\partial x^2} = \frac{\partial^2 \hat{\phi}}{\partial u^2} \end{aligned} \tag{A.11.3}$$

whereby

$$c^2 \frac{\partial^2 \hat{\phi}}{\partial u^2} \equiv c^2 \frac{\partial^2 \hat{\phi}}{\partial u^2}. \tag{A.11.4}$$

Moreover, that the parameter c has units of speed can be seen easily via the unit equation for A.11.2, namely

$$\frac{[\phi]}{[T]^2} = [c]^2 \frac{[\phi]}{[L]^2} \;\rightarrow\; [c]^2 = \frac{[L]^2}{[T]^2} \;\rightarrow [c] = \frac{[L]}{[T]}. \tag{A.11.5}$$

Notwithstanding the interpretive advantage of D'Alembert's solution, one often pursues solutions to the wave equation using the method of separation of variables. That is, we assume that the solution can be written in the form $\phi(x,t) = X(x)T(t)$, whereby we have

$$X\frac{d^2T}{dt^2} = c^2T\frac{d^2X}{dx^2} \quad \rightarrow \quad \frac{1}{T}\frac{d^2T}{dt^2} = \frac{c^2}{X}\frac{d^2X}{dx^2}. \tag{A.11.6}$$

Of course, the only way for a function of time (left hand side) to equal a function of position (right hand side) for all (x,t) is for both functions to equal the same constant, say A. Hence, we have two second order ordinary differential equations to solve, namely

$$\frac{d^2T}{dt^2} = AT, \quad \frac{d^2X}{dx^2} = \frac{A}{c^2}X. \tag{A.11.7}$$

Three solutions are possible depending on whether $A<0$, $A=0$, or $A>0$. It can be shown that $A>0$ and $A=0$ do not lead to periodic solutions and thus are not realistic. If $A<0$, however, one finds solutions for both $X(x)$ and $T(t)$. In this case, it is convenient to let $A \equiv -\lambda^2$ $(\lambda>0)$, whereby the final solution is (Wylie and Barrett 1982)

$$\begin{aligned}\phi(x,t) &= X(x)T(t)\\ &= \left(C_1\cos\frac{\lambda}{c}x + C_2\sin\frac{\lambda}{c}x\right)(C_3\cos\lambda t + C_4\sin\lambda t)\end{aligned} \tag{A.11.8}$$

where C_1, C_2, C_3, C_4 are material parameters to be determined from boundary and initial conditions. Clearly, this solution is periodic for it repeats itself every time t increases by $2\pi/\lambda$. As we close this chapter, similar to Chap. 8, we are reminded that many fundamental approaches of applied mathematics prove essential in solving problems in biomechanics, hence one must commit to studying both.

Exercises

11.1 Repeat the nondimensional analysis of Sect. 11.2 using as length, time, and mass scales:

$$L_s = A, \quad T_s = \frac{A^2H}{Q}, \quad M_s = \rho A^2H.$$

Compare the results with those in Sect. 11.2.

11.2 Repeat Exercise 11.1 using

$$L_s = A, \quad T_s = \sqrt{\frac{\rho A^2}{\Delta p}}, \quad M_s = \rho A^2H.$$

11.3 Recall from Observation 10.3 that the Buckingham Pi method can be used to nondimensionalize known equations. Show that the governing differential equation of motion for the aneurysm [Eq. (11.53)] can be written in nondimensional form as

$$\left(\frac{1}{x^2}+bx\right)\ddot{x}+\frac{3}{2}b\dot{x}^2+4m\frac{\dot{x}}{x}+2\frac{f(x)}{x}=F(\tau),$$

where

$$x\equiv\lambda, \qquad f=\frac{T}{c},$$
$$b=\frac{\rho A}{\rho_s H}, \qquad F=\frac{PA}{c},$$
$$m=\frac{\mu}{\sqrt{\rho_s c H}}, \qquad \tau=\frac{t\sqrt{c}}{\sqrt{\rho_s A^2 H}},$$

and c is a material parameter having units of force/length.

11.4 If the CSF surrounding a spherical aneurysm is assumed to be ideal, then the governing equation reduces to

$$\left(\frac{1}{x^2}+bx\right)\ddot{x}+\frac{3}{2}b\dot{x}^2+2\frac{f(x)}{x}=F(\tau).$$

If $F(\tau)=F_0$, a constant, show that the equation can be integrated once in time to yield

$$\frac{1}{2}\dot{x}^2+\frac{1}{2}b\dot{x}^2x^3+2\int xf(x)dx-\frac{1}{3}F_0x^3=\text{constant}.$$

This form of the equation can be related to the first law of thermodynamics (e.g., $\dot{x}^2/2$ is a nondimensional kinetic energy term, and $-F_0x^3/3$ is a work-type term related to a pressure times volume). Hint: Note that

$$\dot{x}\ddot{x}=\frac{d}{dt}\left(\frac{1}{2}\dot{x}^2\right), \quad x^2\ddot{x}=\frac{d}{dt}\left(\frac{1}{3}x^3\right), \quad dx=\frac{dx}{dt}dt.$$

11.5 If $F(\tau)\equiv F_0$, a constant, if $f(x)=f_0$, a constant surface tension, and if there is no external fluid, then the governing equation of motion of a spherical "soap bubble" is (cf. equation in Exercise 11.3)

$$\frac{1}{x^2}\ddot{x}+\frac{2f_0}{x}=F_0.$$

Solve this equation for $x(\tau)$ and comment on its interpretation.

11.6 In Sect. 11.3, we saw that the pressure field $p(r, t)$ in a radial flow in a spherical domain for an incompressible, Newtonian fluid is independent of the viscosity; that is, we have found a special flow wherein the same pressure field satisfies both the Navier–Stokes and the Euler equations. Because the flow is radial, we can also define a radial streamline $s \equiv r$, where $ds = dr$. Show, therefore, that an unsteady Bernoulli equation can be written in the form

$$p_A + \rho g z_A + \frac{1}{2}\rho v_A^2 = p_B + \rho g z_B + \frac{1}{2}\rho v_B^2 + \rho \int_A^B \frac{\partial v_s}{\partial t} ds.$$

Hint: Integrate the appropriate Euler equation along a radial streamline.

11.7 Use the unsteady Bernoulli equation in Exercise 11.6, with point A at $r = \text{a}$, point B at $r = \infty$, and $v_s \equiv v_r = g(t)/r^2$ from our mass balance relation, to show that one obtains the same pressure field $p(r, t)$ from Bernoulli as obtained from Navier–Stokes.

11.8 Repeat Example 11.3 for $\eta = 0.0625$, $\zeta = -0.1$, $c = 1.0$, $\alpha = 0.5$, $F(t) = 1.0 \sin t$, $x(0) = 0$, and $\dot{x}(0) = 1$. What does the negative value of ζ induce?

11.9 Repeat Exercise 11.8 with $x(0) = 1$ and $\dot{x}(0) = 1$.

11.10 Viscoelastic characteristics include instantaneous elasticity, creep, stress relaxation, instantaneous recovery, delayed elasticity, permanent set, and hysteresis. Define and discuss each characteristic.

11.11 We found in Eq. (11.59) that the stress relaxation $\sigma(t)$ in a Maxwell model is given by an exponential decay. Compute the rate of change of stress as a function of time. Observe that the relaxation is initially very rapid; indeed, show that only 37 % of the initial stress remains at time $t = t_R$, the relaxation time.

11.12 Similar to the previous exercise, investigate the creep response of a Kelvin–Voigt model. In particular, compute $\dot{\varepsilon}(t)$ and sketch it versus time. Show, too, that only 37 % of the asymptotic strains remains to be realized after $t = t_c$.

11.13 As we saw in Eq. (11.64), the Kelvin–Voigt model does not allow stress relaxation. Intuitively, we realize that a step change in ε from 0 to ε_0 at time $t = 0$ can only be accomplished via an infinite stress (if that were possible) because a viscous dashpot cannot otherwise extend instantaneously. Thereafter, the stress in the viscous element drops to zero, for it requires a strain rate to produce a stress, thus the spring sustains the constant extension with a constant stress. In a similar way, qualitatively discuss the creep response of the Kelvin–Voigt model and, in particular, justify why this behavior is sometimes referred to as a *delayed elasticity* (cf. Findley et al. 1976, p. 56).

11.14 Recall again the stress relaxation of a Maxwell model:

$$\sigma(t) = \sigma_0 e^{-t/t_R},$$

where t_R is the so-called relaxation time. Because the model is linear, superposition holds (cf. Sect. 5.5 of Chap. 5). Thus, a set of Maxwell models in parallel (Fig. 11.26) and under a constant strain ε_0 will stress relax according to

$$\sigma(t) = \varepsilon_0 \sum_{i=1}^{n} E_i e^{-t/t_R^i},$$

where $t_R^i = \mu_i/E_i$ for all elements $i = 1, 2, \ldots n$. For a continuous distribution of relaxation times, from 0 to ∞, we have

$$\sigma(t) = \varepsilon_0 \int_0^\infty R(t_R) e^{-t/t_R} dt_R,$$

where $R(t_R)$ is called the *relaxation spectrum*—a distribution of relaxation times. Formulate a similar analysis of the creep response of a set of Kelvin–Voigt elements in series whereby

$$\varepsilon(t) = \sigma_0 \sum_{i=1}^{n} C_i \left(1 - e^{-t/t_c^i}\right),$$

or

$$\varepsilon(t) = \sigma_0 \int_0^\infty C(t_c) \left(1 - e^{-t/t_c}\right) dt_c,$$

where $C(t_c)$ is called the retardation spectrum.

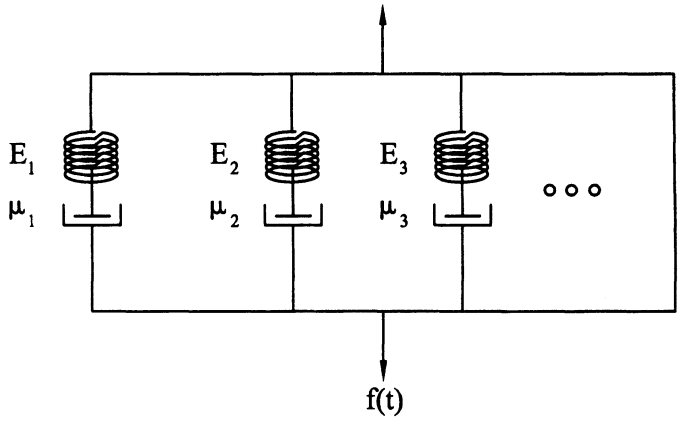

FIGURE 11.26

11.15 A Maxwell model in series with a Kelvin–Voigt model is a four-parameter model sometimes called a *Burgers* model. If the spring stiffness and dashpot viscosity are given by (E_1, μ_1) and (E_2, μ_2) for the Maxwell and Kelvin–Voigt components, respectively, show that the creep function (or compliance) for the Burgers model is

$$J(t) = \frac{1}{E_1} + \frac{t}{\mu_1} + \frac{1}{E_2}\left(1 - e^{-E_2 t/\mu_2}\right).$$

11.16 Assume that a uniaxial member is subjected to a strain of the form $\varepsilon(t) = \varepsilon_A \sin \omega t$. If the material behaves elastically, one would expect a stress response of the form $\sigma(t) = \sigma_A \sin \omega t$ (i.e., in phase). For a viscoelastic response, however, one would expect the stress response to be out of phase with the strain. Hence, let

$$\sigma(t) = \sigma_A \sin(\omega t + \phi) = \sigma_A(\sin \omega t \cos \phi + \cos \omega t \sin \phi),$$

where ϕ is the phase angle. This form suggests that a complex representation may be useful, namely

$$\varepsilon(t) = \varepsilon_A e^{i\omega t}, \quad \sigma(t) = \sigma_A e^{i(\omega t + \phi)},$$

where $i = \sqrt{-1}$. Show that

$$\frac{\sigma(t)}{\varepsilon(t)} = \frac{\sigma_A}{\varepsilon_A} e^{i\phi} = G_1 + iG_2,$$

where G_1 and G_2 are called the *storage modulus* and the *loss modulus,* respectively. Show, too, that

$$G_1 = \frac{\sigma_A}{\varepsilon_A}\cos\phi, \quad G_2 = \frac{\sigma_A}{\varepsilon_A}\sin\phi, \quad \tan\phi = \frac{G_2}{G_1}.$$

Note that, for example, $G_1 \sim 10^9$ Pa, $G_2 \sim 10^7$ Pa, and $\phi \sim 0.01$ for a typical polymer.

11.17 Following up on Exercise 11.16, note that $G^* = G_1 + iG_2$ is called the *complex modulus*. Show that for the sinusoidal straining in Exercise 11.16, the magnitude of $G^* = \sigma_A/\varepsilon_A$. Note, too, that $\tan\phi$ is often called the *mechanical loss*.

11.18 If a Standard model consists of a spring in series with a Kelvin–Voigt element, and the spring has a stiffness $E = 1$ GPa, whereas the Kelvin–Voigt element has stiffness 10 kPa and viscosity 10^7 P (poise), plot $\log J_1$, $\log J_2$, and $\log(\tan\phi)$ versus $\log\omega \in [-8, 8]$, where

$$J^* = J_1 - iJ_2 = \frac{\varepsilon_0}{\sigma_0} e^{-i\phi}$$

for creep.

11.19 Show that for a Maxwell model subjected to an oscillatory motion,

$$G^* = \frac{\mu^2\omega^2/E}{1+\mu^2\omega^2/E^2} + i\left(\frac{\mu\omega}{1+\mu^2\omega^2/E^2}\right)$$

and

$$\tan\phi = \frac{G_2}{G_1} = \frac{E}{\omega\mu}.$$

11.20 Consistent with the prior exercise, plot $\tan\phi$ and $|G^*|$ versus $\log\omega \in [-4, 4]$ given values of $E = 1$ GPa and $\mu = 5 \times 10^9$ P. Repeat for the same E but with $\mu = 5 \times 10^{10}$ then 5×10^8 P. Discuss the behavior in terms of changes in t_R. Note that these values are reasonable for a polymer that may be used in a biomedical device.

11.21 Show that the frictional drag coefficient C_f for the step-slider in Sect. 11.5.2 is correct as given. Hint: The total drag force F_D can be computed by integrating the shear stresses over the bearing surface; that is,

$$F_D = w\int_0^{L(1-b)} \tau_1 dx_1 + \int_{L(1-b)}^{bL} \tau_2 dx_2,$$

where, in general,

$$\tau \equiv \mu \left.\frac{\partial v_x}{dy}\right|_{y=0}$$

11.22 The so-called *Reynolds' equation* governs general flows in hydrodynamic lubrication theory. In one dimension, show that it can be written as

$$\frac{d}{dx}\left(\frac{h^3(x)w}{\mu}\left(\frac{dp}{dx}\right)\right) + 6U\frac{dh}{dx} = 0.$$

Hint: Use the result for the velocity $v_x(y)$ in Sect. 11.5.2 and compute the volumetric flow rate

$$Q = w\int_0^{h(x)} v_x(y)dy.$$

Exploit the fact that Q is constant with respect to x even though the gap distance is $h = h(x)$.

11.23 Although the Moens-Korteweg equation is theoretically inappropriate for use in arterial mechanics, it provides correct order of magnitude results nonetheless. If $\rho \sim 1{,}060$ kg/m^3 for blood and $E \sim 1$ MPa and $h/a \sim 0.1$ for an artery, estimate the speed of a pressure wave and compare to values measured clinically in a human aorta. Discuss in a 2-page report the implications of increased arterial stiffening with aging and associated increases in the so-called pulse wave velocity (PWV).

11.24 Because of the complexity of fluid-solid interactions in the vasculature, sophisticated computational methods must be used to study issues such as the effects of wall stiffness on pressure waves. Discuss in a 2-page report recent advances and associated computational findings regarding regional pulse wave velocities in humans and changes therein due to aging. As a start, see the paper by Xiao N. et al. (2013) Computer simulation of blood flow, pressure, and vessel wall dynamics in a full-body-scale three dimensional model of the human vasculature. *J Comp Phys* 244: 22-40.

11.25 Discuss in a 2-page report the utility of "dynamic similarity" in the design of medical devices that are deployed within the vasculature.